Oncogene (2005) 24, 938–944

www.nature.com/onc

Protein stability and function of p73 are modulated by a physical interaction with RanBPM in mammalian cultured cells

Sonja Kramer[1], Toshinori Ozaki[1], Kou Miyazaki[1], Chiaki Kato[1], Takayuki Hanamoto[1] and Akira Nakagawara*,[1]

[1]*Division of Biochemistry, Chiba Cancer Center Research Institute, 666-2 Nitona, Chuoh-ku, Chiba 260-8717, Japan*

Upon a certain DNA damage including cisplatin treatment, p73 is stabilized and exerts its growth-suppressive and/or proapoptotic function. However, the precise molecular basis by which the intracellular levels of p73 are regulated remains unclear. In the present study, we have identified RanBPM as a novel binding partner of p73α by yeast-based two-hybrid screening, and also found that RanBPM has an ability to stabilize p73α. GST pull-down assays and co-immunoprecipitation experiments revealed that RanBPM directly bound to the extreme COOH-terminal region of p73α, whereas it failed to interact with p53. Co-expression of RanBPM with p73α resulted in the nuclear translocation of RanBPM, and both proteins co-localized in cell nucleus as examined by indirect immunofluorescent staining. It is worth noting that the expression of RanBPM inhibited the ubiquitination of p73α, and thereby prolonged its half-life. Subsequent studies demonstrated that the proapoptotic activity of p73α was significantly enhanced in the presence of RanBPM. Taken together, our present findings implicate a novel role for RanBPM in the regulation of p73 stability and function.
Oncogene (2005) **24**, 938–944. doi:10.1038/sj.onc.1208257
Published online 22 November 2004

Keywords: p53; p73; RanBPM; two-hybrid; ubiquitination

p73 is a newly identified p53-related nuclear transcription factor, and functions to promote cell cycle arrest and/or apoptosis (Kaghad *et al.*, 1997). These cellular roles of p73 are largely attributed to its ability to transactivate specific target genes. In contrast to p53, p73 is expressed as multiple isoforms arising from either alternative splicing or alternative promoter usage (Melino *et al.*, 2002). Although functional differences among the splicing isoforms with different COOH-termini remain unclear, NH_2-terminally truncated forms of p73 (ΔNp73) have an oncogenic potential and exhibit a dominant-negative behavior toward wild-type p73 as well as p53 (Pozniak *et al.*, 2000; Nakagawa *et al.*, 2002; Stiewe *et al.*, 2002).

Steady-state levels of p73 are kept extremely low under normal conditions, however, p73 is significantly induced at protein level in response to a certain genotoxic stress including cisplatin treatment, which is mediated by a nuclear nonreceptor tyrosine kinase c-Abl (Agami *et al.*, 1999; Gong *et al.*, 1999; Yuan *et al.*, 1999). c-Abl binds to the PXXP motif of p73 and phosphorylates p73 at Tyr-99. Alternatively, Ren *et al.* (2002) reported that protein kinase Cδ catalytic fragment phosphorylates p73 at Ser-289, and increases its stability, suggesting that post-translational modification such as phosphorylation might contribute to increase the stability of p73. Protein phosphorylation has been shown to be involved in the initiation of protein ubiquitination by E3 ubiquitin ligase (Carrano *et al.*, 1999; Ganoth *et al.*, 2001). As described previously (Balint *et al.*, 1999; Lee and La Thangue, 1999), p73 is regulated at least in part by the protein degradation process through the ubiquitin–proteasome system. Additionally, Lee and La Thangue (1999) described that the COOH-terminal region of p73α might have a regulatory role in the proteasome-dependent degradation of p73. Recently, we have found that MM1 and RACK1 interact with the extreme COOH-terminal region of p73α, and regulate its transcriptional activity as well as proapoptotic function (Watanabe *et al.*, 2002; Ozaki *et al.*, 2003). However, these interactions did not have a detectable effect on the intracellular levels of p73α.

To identify the possible cellular protein(s) involved in the regulation of p73 protein stability, we screened a cDNA library derived from human fetal brain using the extreme COOH-terminal region of p73α (amino-acid residues 551–636) as a bait in a yeast-based two-hybrid system. After screening of approximately 5×10^5 transformants, 12 independent clones exhibited a high level of β-galactosidase activity, and subsequent sequence analysis revealed that three out of them encoded the overlapping regions of RanBPM (Figure 1a). RanBPM was initially identified as a cellular protein that can interact with Ran nuclear–cytoplasmic transport protein (Nakamura *et al.*, 1998; Nishitani *et al.*, 2001), and contained the putative SPRY domain which might be involved in protein–protein interactions (Ponting *et al.*, 1997). Although most of the Ran-binding proteins play an important role in nucleocytoplasmic transport, it is

*Correspondence: A Nakagawara;
E-mail: akiranak@chiba-ccri.chuo.chiba.jp
Received 16 July 2004; revised 4 October 2004; accepted 6 October 2004; published online 22 November 2004

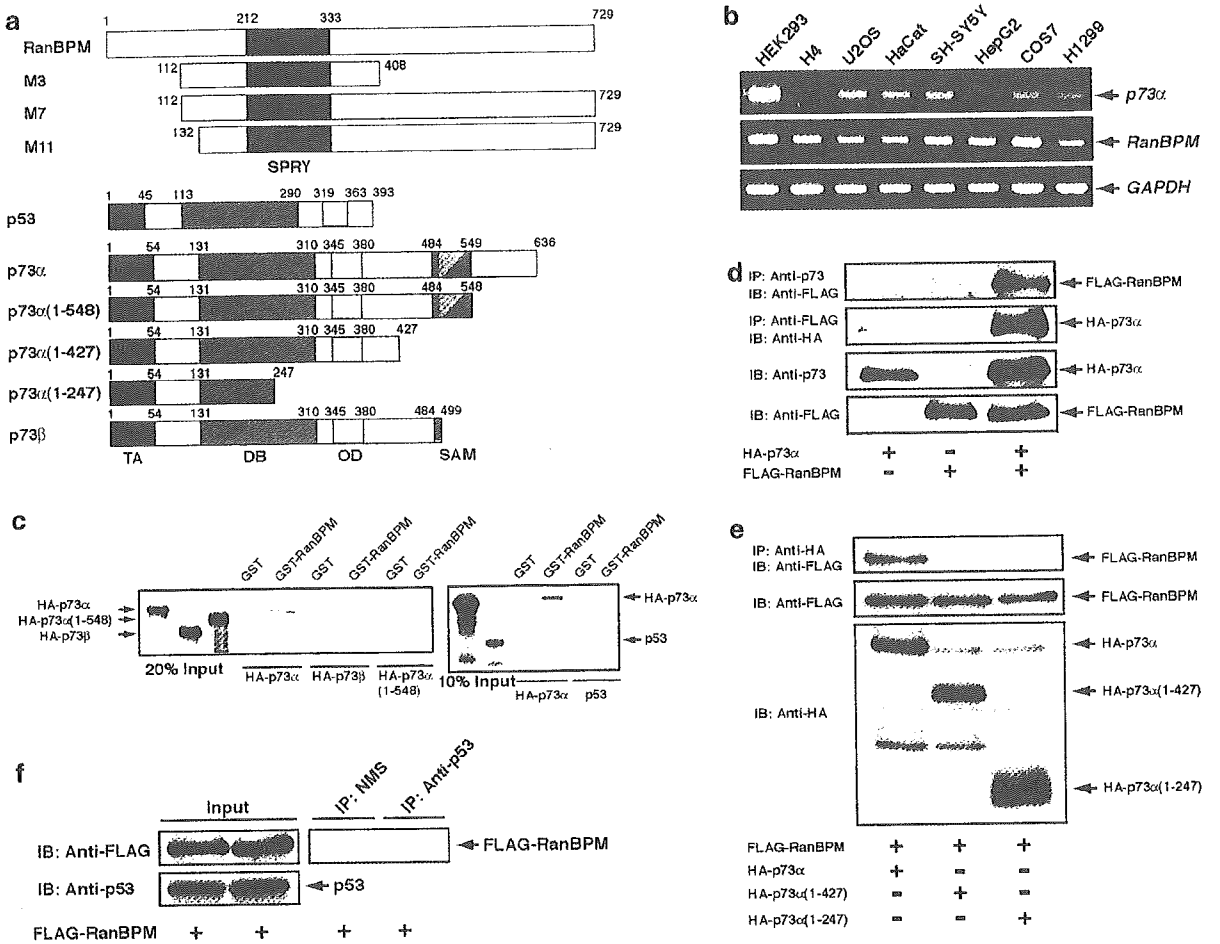

Figure 1 Identification of RanBPM as a binding partner of p73. (**a**) The three overlapping RanBPM clones (M3, M7 and M11) isolated from the yeast two-hybrid screening along with the full-length RanBPM are shown. The putative SPRY domain (amino-acid residues 212–333) is indicated. Structures of p73 and p53 are also shown. TA, transactivation domain; DB, DNA-binding domain; OD, oligomerization domain; SAM, sterile α motif domain. Amino-acid numbering was relative to first methionine, which represents position +1. (**b**) Expression of *RanBPM* and *p73*. Total RNA prepared from the indicated cell lines were incubated with SuperScript II reverse transcriptase (Invitrogen, Carlsbad, CA, USA), and generated cDNAs were amplified by PCR in the presence of primers specific for *p73* (top panel), *RanBPM* (middle panel) or *GAPDH* (bottom panel). (**c**) GST pull-down assay. *In vitro* translated ^{35}S-labeled p73α, p73β, p73α (1–548) or p53 was incubated with bacterially expressed GST or GST-RanBPM(112–408) for 2 h at 4°C. Bound complexes were recovered on the glutathione–sepharose beads (Amersham Pharmacia Biotech, Piscataway, NJ, USA), washed extensively with the binding buffer (50 mM Tris–HCl, pH 7.5, 150 mM NaCl, 0.1% Nonidet P-40, 1 mM EDTA, and 1 mM phenylmethylsulfonyl fluoride), and then boiled in SDS sample buffer. Bound proteins were resolved by 10% SDS–polyacrylamide gel, and analysed by autoradiography. The input of the radio-labeled proteins used in the binding reaction is also shown. (**d**) p73α interacts with RanBPM in mammalian cultured cells. COS7 cells transfected with the indicated expression plasmids were lysed in 25 mM Tris–HCl, pH 8.0, 137 mM NaCl, 1% Triton X-100 and 1 mM phenylmethylsulfonyl fluoride. Whole-cell lysates were immunoprecipitated with anti-p73 antibody (Ab-4, NeoMarkers, Fremont, CA, USA) or anti-FLAG (M2, Sigma, St Louis, MO, USA), and subjected to immunoblotting with anti-FLAG (first panel) or with anti-HA (12CA5, Roche Molecular Biochemicals, Indianapolis, IN, USA) antibody (second panel), respectively. Separate aliquots of the lysates were immunoblotted with anti-p73 (third panel) or anti-FLAG antibody (fourth panel) to confirm the expression of FLAG-RanBPM or HA-p73α, respectively. (**e**) COOH-terminal region of p73α is required for the interaction with RanBPM. COS7 cells were co-transfected with the indicated combinations of the expression plasmids, and whole-cell lysates were immunoprecipitated with anti-HA antibody, followed by immunoblotting with anti-FLAG antibody (top panel). Cell lysates were immunoblotted as a control for FLAG-RanBPM (middle panel), HA-p73α and HA-p73α derivatives (bottom panel) in the input lysate. (**f**) p53 does not bind to RanBPM. Cell lysates prepared from COS7 cells transfected with FLAG-RanBPM were immunoprecipitated with the normal mouse serum (NMS, Jackson ImmunoResearch Laboratories, West Grove, PA, USA) or anti-p53 antibodies (DO-1 plus PAb1801, Oncogene Research Products, Cambridge, MA, USA). Immunoprecipitates were analysed by immunoblotting with anti-FLAG antibody (right panel). Left panels show the Western blotting with anti-FLAG, or anti-p53 antibody to monitor the expression level of FLAG-RanBPM or the endogenous p53, respectively

unlikely that RanBPM is involved in this process (Nishitani *et al*., 2001). Alternatively, Nakamura *et al*. (1998) reported that RanBPM might be involved in reorganization of the microtubule network; however, the precise function of RanBPM remains unknown.

Consistent with the previous observations (Rao *et al*., 2002), *RanBPM* was expressed in various cell lines (Figure 1b). To confirm the interaction between RanBPM and p73, we performed GST pull-down assays using a GST fusion protein containing RanBPM

(112–408) and *in vitro* translated ^{35}S-labeled p73α, p73β, p73α(1–548) or p53. GST alone was employed as a negative control. As shown in Figure 1c, radio-labeled p73α was pulled down by GST-RanBPM(112–408) but not by GST alone. However, p73β and p73α(1–548), which lack the extreme COOH-terminal portion of p73α, were no longer able to interact with GST-RanBPM(112–408). In addition, p53 failed to bind to GST-RanBPM(112–408). In good agreement with the yeast two-hybrid results, these observations suggest that the extreme COOH-terminal portion of p73α is responsible for the physical interaction with RanBPM. Next, we performed co-immunoprecipitation experiments to confirm their interaction in cells. To this end, cell lysates prepared from COS7 cells co-transfected with HA-tagged p73α and FLAG-tagged full-length RanBPM were immunoprecipitated with anti-p73 or anti-FLAG antibody, followed by immunoblotting with anti-FLAG or anti-HA antibody, respectively. As shown in Figure 1d, HA-p73α co-immunoprecipitated with FLAG-RanBPM. Under our experimental conditions, HA-p73α(1–427) and HA-p73α(1–247) did not co-immunoprecipitate with FLAG-RanBPM (Figure 1e). In contrast to full-length p73α, the anti-p53 immunoprecipitates did not contain FLAG-RanBPM (Figure 1f). Taken together, our results suggest that RanBPM has an ability to interact with p73α but not with p53 in mammalian cultured cells.

Previous immunostaining studies have shown that p73α is exclusively localized in cell nucleus (Jost *et al.*, 1997), while RanBPM could distribute to the cell nucleus, perinuclear region and cytoplasm (Nishitani *et al.*, 2001; Umeda *et al.*, 2003). To examine the subcellular localization of RanBPM in the presence or absence of p73α, COS7 cells were transfected with the indicated expression plasmids, and the indirect immunofluorescent staining was performed. As shown in Figure 2a and b, FLAG-RanBPM and HA-p73α were detected largely in the cytoplasm and cell nucleus, respectively. Of note, when FALG-RanBPM was co-expressed with HA-p73α, a fraction of FLAG-RanBPM translocated into cell nucleus, and co-localized with nuclear HA-p73α (Figure 2c–e). To confirm this issue, transfected COS7 cells were fractionated into nuclear and cytoplasmic fractions, and their subcellular localizations were analysed by immunoblotting. The purity of the nuclear and cytoplasmic fractions was examined by immunoblotting with anti-Lamin B and anti-α-tubulin antibody, respectively. Consistent with the indirect immunofluorescent staining, co-expression of FLAG-RanBPM with HA-p73α resulted in a significant nuclear accumulation of FLAG-RanBPM, whereas FLAG-RanBPM alone was detected in the cytoplasmic fraction (Figure 2f). In addition, the amounts of nuclear HA-p73α seemed to be increased in the presence of FLAG-RanBPM. It is thus likely that RanBPM interacts with p73α in cell nucleus, and could affect the stability of p73α.

To test whether RanBPM could affect the stability of p73α, COS7 cells were co-transfected with the constant amount of HA-p73α together with or without the

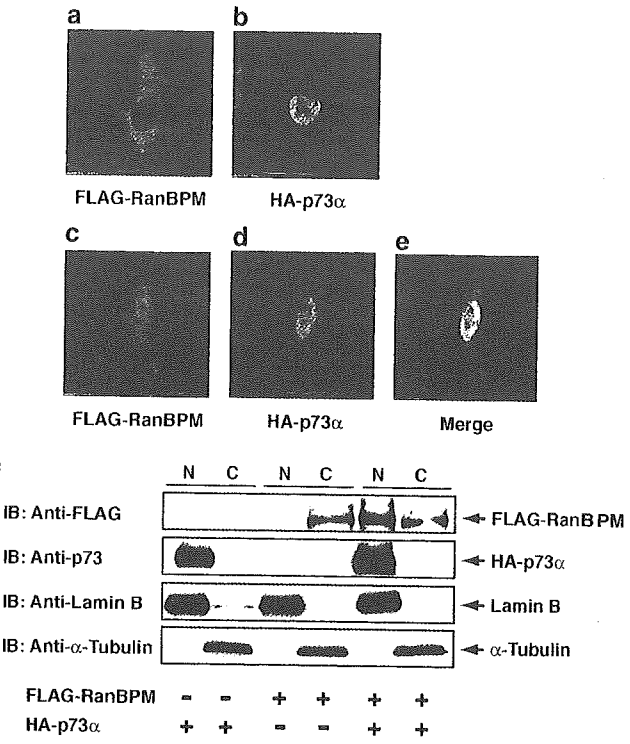

Figure 2 Subcellular distribution of RanBPM in the presence of p73. (**a–e**) Nuclear co-localization of p73α and RanBPM by immunofluorescence. COS7 cells were transfected with FLAG-RanBPM (**a**), HA-p73α (**b**) or FLAG-RanBPM and HA-p73α (**c–e**). At 48 h after transfection, cells were fixed in 20% methanol and incubated with anti-FLAG (red) and anti-HA antibody (green) (Medical and Biological Laboratories, Nagoya, Japan), followed by the incubation with the rhodamine- and FITC-conjugated secondary antibodies (Jackson ImmunoResearch Laboratories), respectively. Cells were then examined under a confocal scanning laser microscope. The merged images of the two signals are displayed in yellow (**e**). (**f**) Fractionation of COS7 cell extracts. COS7 cells were transfected with the indicated expression plasmids. At 48 h after transfection, cells were fractionated into nuclear (N) and cytoplasmic (C) fractions, and then analysed directly by immunoblotting with anti-FLAG (first panel) or anti-p73 antibody (second panel). The nuclear or cytoplasmic fraction was confirmed by immunoblotting with anti-Lamin B (Ab-1, Oncogene Research Products) (third panel) or anti-α-tubulin antibody (DM1A, Cell Signaling Technology, Beverly, MA, USA) (fourth panel), respectively

increasing amounts of FLAG-RanBPM. As shown in Figure 3a, the amount of HA-p73α was markedly increased in the presence of FLAG-RanBPM in a dose-dependent manner, whereas the expression level of p73α mRNA remained unchanged. On the other hand, FLAG-RanBPM had no significant effect on the levels of exogenous p53 (Figure 3b). Similar results were also obtained in p53-deficient H1299 cells (data not shown). We next sought to determine the half-life of p73α in the presence of RanBPM. For this purpose, COS7 cells were transfected with HA-p73α together with or without FLAG-RanBPM. At 24 h after transfection, cells were treated with cycloheximide. At the indicated time periods, cell lysates were analysed for HA-p73α by immunoblotting. In accordance with the previous reports (Lee and La Thangue, 1999; Ohtsuka *et al.*,

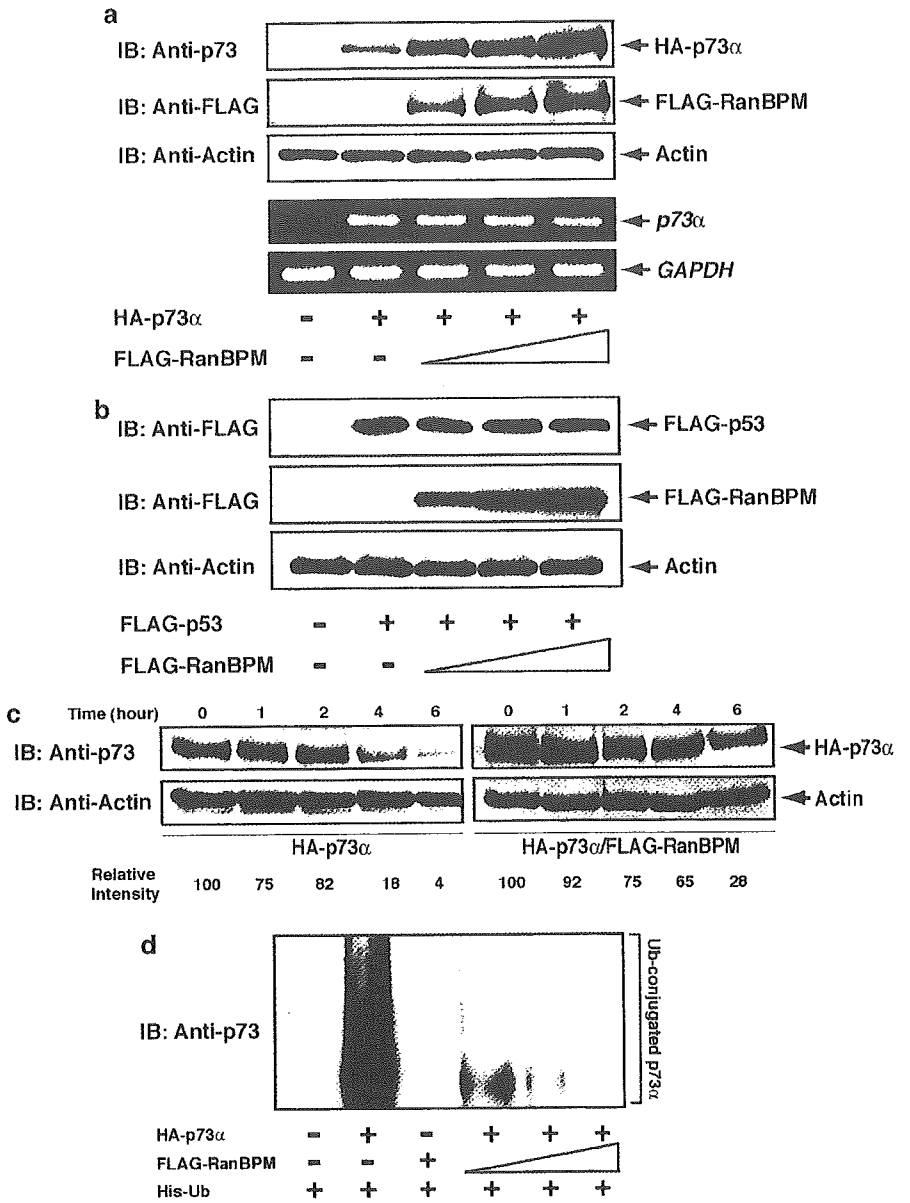

Figure 3 RanBPM increases the stability of p73 but not of p53. (**a**) RanBPM increases the amounts of p73α. COS7 cells were co-transfected with the constant amount of HA-p73α (0.5 μg) together with or without the increasing amounts of FLAG-RanBPM (0.5, 1.0 and 1.5 μg). The total amount of plasmid DNA was kept constant (2 μg) with pcDNA3. At 48 h after transfection, cell lysates or total RNA were prepared, and subjected to immunoblotting with the indicated antibodies (upper panels) or RT–PCR analysis (lower panels). Immunoblotting for actin (20–33, Sigma Chemical Co.) serves as a loading control. (**b**) RanBPM does not affect the amounts of p53. COS7 cells were co-transfected with the indicated combinations of the expression plasmids, and were processed for immunoblotting as described above. (**c**) RanBPM increases the half-life of p73α. COS7 cells were transfected with HA-p73α alone (0.5 μg) (left panels) or together with FLAG-RanBPM (1.5 μg) (right panels). At 24 h post-transfection, cells were treated with cycloheximide (100 μg/ml) and harvested at the indicated time periods. Cell lysates were used for immunoblotting with the indicated antibodies. The intensity of the bands was quantified by using densitometry. (**d**) RanBPM inhibits the ubiquitination of p73α. COS7 cells were co-transfected with the constant amount of HA-p73α (0.5 μg) and His-tagged ubiquitin (Ub) (0.5 μg), together with or without the increasing amounts of FLAG-RanBPM (0.5, 1.0 and 1.5 μg). At 24 h post-transfection, cells were treated with 20 μM MG-132 for 6 h before being harvested. His-tagged ubiquitin-containing protein complexes were pulled down with Ni^{2+}-agarose beads (QIAGEN, Valencia, CA, USA), and subsequently resolved by 10% SDS–polyacrylamide gel electrophoresis, followed by immunoblotting with anti-p73 antibody

2003), ectopically expressed p73α had a half-life of less than 4 h, whereas the degradation rate of HA-p73α was slower in FLAG-RanBPM-expressing cells (Figure 3c). Thus, it is likely that the RanBPM-dependent stabilization of p73α is attributed to the clear increase in the half-life of p73α.

As described (Balint *et al*., 1999), the stability of p73 is regulated at least in part through the ubiquitin–proteasome pathway. These observations prompted us to determine whether RanBPM could prevent the ubiquitination of p73. COS7 cells were transfected with HA-p73α- and His-tagged ubiquitin, or in combination

with the increasing amounts of FLAG-RanBPM. At 24 h after transfection, cells were treated with MG-132 for 6 h. His-ubiquitinated proteins were purified by Ni^{2+}-agarose beads, and then analysed by immunoblotting with the anti-p73 antibody. As shown in Figure 3d, the slower migrating ubiquitinated forms of p73α were detectable in the absence of FLAG-RanBPM. Intriguingly, the ubiquitination levels of p73α were significantly reduced in cells expressing FLAG-RanBPM, suggesting that RanBPM stabilizes p73α by inhibiting its ubiquitination.

To determine whether RanBPM could affect the transcriptional activity of p73α, H1299 cells were transiently transfected with a constant amount of the expression plasmid for HA-p73α, together with the p53/p73-responsive $p21^{WAF1}$ or *MDM2* luciferase reporter constructs in the presence or absence of increasing amounts of the FLAG-RanBPM expression plasmid. As shown in Figure 4a, expression of FLAG-RanBPM enhanced the ability of p73α to transactivate the $p21^{WAF1}$ and *MDM2* promoters in a dose-dependent manner. To extend the functional significance of their interaction, we examined the possible effect of RanBPM on the p73α-mediated apoptosis. H1299 cells were transfected with HA-p73α, FLAG-RanBPM, or HA-p73α and FLAG-RanBPM. The β-galactosidase was used as a marker to visualize the transfected cells. At 48 h post transfection, the number of β-galactosidase-positive cells was scored. As shown in Figure 4b, the number of β-galactosidase-positive cells expressing FLAG-RanBPM was similar to that detected in the empty plasmid-transfected cells. Consistent with the previous report (Watanabe *et al.*, 2002), expression of HA-p73α resulted in a clear decrease in the number of β-galactosidase-positive cells. Of note, co-expression of HA-p73α with FLAG-RanBPM significantly reduced the number of β-galactosidase-positive cells as compared with that observed in cells expressing HA-p73α alone. In addition, we performed a colony formation assay. H1299 cells were transfected with HA-p73α, FLAG-RanBPM or HA-p73α plus FLAG-RanBPM, and the transfected cells were selected in the presence of G418. After 2 weeks of selection, drug-resistant colonies were fixed and stained with Giemsa's solution. In accordance with the β-galactosidase assay, FLAG-RanBPM expression did not affect the colony formation as compared with the empty plasmid-transfected control, whereas co-expression of HA-p73α with FLAG-RanBPM reduced the colony formation even more efficiently than HA-p73α alone (Figure 4c). Considering that p73α efficiently induced apoptosis in H1299 cells (Di Como *et al.*, 1999; Zeng *et al.*, 1999), these results suggest that RanBPM increases the proapoptotic activity of p73α. To further confirm this issue, H1299 cells were transiently transfected with a constant amount of the GFP expression plasmid along with the indicated combinations of the expression plasmids. At 48 h after transfection, transfected cells were identified by fluorescence microscopy for the appearance of green fluorescence, and the number of GFP-positive cells with condensed and fragmented nuclei was counted. As shown in Figure 4d, co-expression of HA-p73α with FLAG-RanBPM increased the number of apoptotic cells as compared with that resulting from expression of HA-p73α alone. Taken together, our present results strongly suggest that RanBPM-mediated stabilization of p73α is critical for its effects on transcriptional activation as well as apoptosis.

Recently, it has been shown that a variety of cellular proteins could interact with RanBPM, including MET, androgen receptor, HIPK2, USP11, Twa1, calbindin D28K and $p75^{NTR}$, suggesting that RanBPM is involved in diverse biological processes (Ideguchi *et al.*, 2002; Rao *et al.*, 2002; Wang D *et al.*, 2002; Wang Y *et al.*, 2002; Bai *et al.*, 2003; Lutz *et al.*, 2003; Umeda *et al.*, 2003). In the present study, we demonstrated that RanBPM increased the stability of p73α by reducing its ubiquitination levels. An important question raised by our results is how RanBPM stabilize p73α. Intriguingly, Ideguchi *et al.* (2002) described that RanBPM is associated with the deubiquitination enzyme USP11, which belongs to the ubiquitin hydrolase family. Considering that p53 is stabilized by direct deubiquitination by the deubiquitination enzyme HAUSP (Li *et al.*, 2002), it is likely that RanBPM could bind to USP11 and promote deubiquitination of p73α by recruiting USP11 to p73α; however, further studies will be required to determine this issue.

Alternatively, Lee and La Thangue (1999) found that p73β is much more stable than p73α, suggesting that the unique COOH-terminal portion of p73α might be critical for degradation by the ubiquitin–proteasome system. According to our present results, RanBPM bound to p73α through its extreme COOH-terminal region, whereas it failed to interact with p73β. Thus, it is plausible that RanBPM might increase the steady-state levels of p73α by masking p73α COOH-terminal lysine residues, which could be the sites for ubiquitin ligation, and/or disrupting the interaction of p73α with unknown proteins required for ubiquitination-mediated proteolysis. These possibilities are currently under investigation. Elucidation of the detailed molecular mechanism underlying the RanBPM-dependent stabilization of p73α would be necessary for better understanding of p73 turnover.

Another finding of the present study is that, under our experimental conditions, cytoplasmic RanBPM became nuclear in the presence of p73α overexpression. Given that RanBPM is localized in both the cytoplasm and nucleus (Nakamura *et al.*, 1998; Nishitani *et al.*, 2001), it is probable that p73α might have an ability to promote nuclear translocation of RanBPM through the physical interaction between them. As described previously, wild-type p53 is predominantly localized in the cytoplasm of many neuroblastoma cells (Moll *et al.*, 1996). The abnormal cytoplasmic distribution of p53 might be attributed at least in part to the interaction with Parc, which acts as a cytoplasmic anchor protein for p53 (Nikolaev *et al.*, 2003). Interestingly, Goldschneider *et al.* (2004) found that enforced expression of p73α in neuroblastoma-derived SH-SY5Y cells significantly enhances the nuclear accumulation of wild-type p53 and

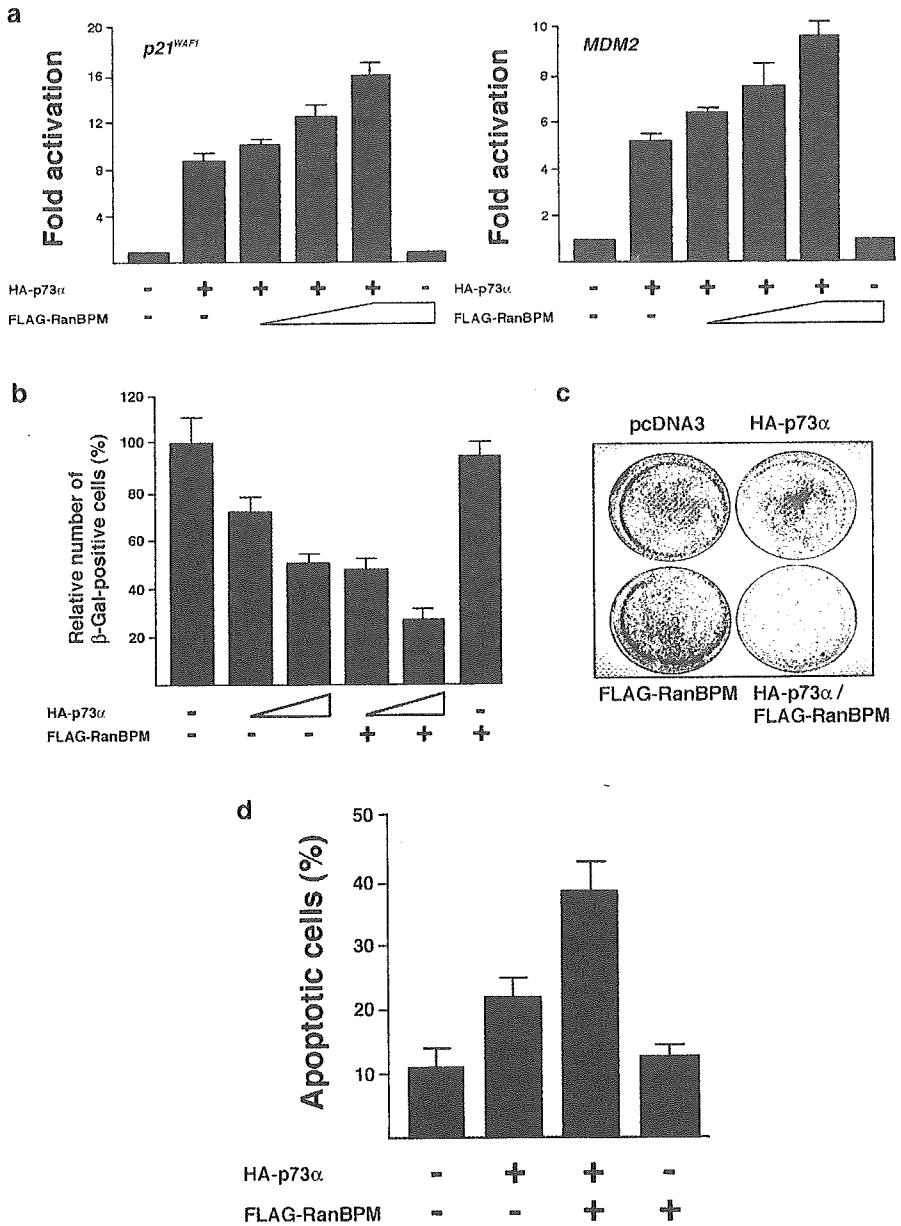

Figure 4 RanBPM enhances p73 function. (**a**) RanBPM enhances the transcriptional activity of p73α. p53-deficient H1299 cells were co-transfected with 25 ng of the expression plasmid for HA-p73α together with 100 ng of p53/p73-responsive *p21*^{WAF1} (left panel) or *MDM2* (right panel) luciferase reporter construct, and 10 ng of the *Renilla* luciferase plasmid (pRL-TK, Promega Corp., Madison, WI, USA), in the presence or absence of increasing amounts of the FLAG-RanBPM expression plasmid (25, 50, or 100 ng). At 48 h after transfection, cells were lysed and their luciferase activities were measured. Firefly luminescence signal was normalized based on the *Renilla* luminescence signal. (**b**) RanBPM stimulates the p73α-mediated growth suppression. H1299 cells were co-transfected with the indicated combinations of the expression plasmid together with the constant amount of the expression plasmid for β-galactosidase (125 ng) (pCH110, Amersham Pharmacia Biotech). At 48 h after transfection, transfected cells were identified by staining with 5-bromo-4-chloro-3-indolyl-β-D-galactopyranoside (X-gal). The relative percentage of β-gal-positive cells represents the ratio of the number of β-gal-positive cells to that of those transfected with pcDNA3 alone. (**c**) Colony formation assay. H1299 cells were transfected with HA-p73α (200 ng), FLAG-RanBPM (750 ng) or HA-p73α (200 ng) plus FLAG-RanBPM (750 ng). Total amount of plasmid DNA was kept constant (1 μg) with pcDNA3, and pcDNA3 alone was used as a negative control. At 2 days after transfection, cells were selected with G418 (400 μg/ml) for 2 weeks. G418-resistant colonies were fixed in methanol, and stained with Giemsa's solution. Representative dishes of three independent experiments are shown. (**d**) RanBPM enhances the p73α-mediated apoptosis. H1299 cells transfected with 0.2 μg of the GFP expression plasmid and 0.5 μg of the HA-p73α expression plasmid together with or without 1.5 μg of the FLAG-RanBPM expression plasmid. At 48 h after transfection, transfected cells were identified by the presence of green fluorescence. Cell nucleus was stained with DAPI to reveal nuclear condensation and fragmentation. The number of GFP-positive cells with apoptotic nuclei was scored

restores its function, indicating that p73α displaces p53 from the cytoplasmic complex containing Parc. It is thus likely that p73α could modulate cellular proteins/pathways that specifically regulate nuclear import and export of RanBPM. Since RanBPM is associated with a variety of nuclear proteins, p73α might play a critical role in regulating nuclear function of RanBPM.

Acknowledgements
We are grateful to Dr S Sakiyama for helpful discussion. This work was supported in part by a Grant-in-Aid from the Ministry of Health and Welfare for a New 10-Year Strategy for Cancer Control, a Grant-in-Aid for Scientific Research on Priority Areas, a Grant-in-Aid for Scientific Research (B) from the Ministry of Education, Science, Sports and Culture, Japan, and a found from the Hisamitsu Pharmaceutical Company.

References

Agami R, Blandino G, Oren M and Shaul Y. (1999). *Nature*, **399**, 809–813.
Bai D, Chen H and Huang BR. (2003). *Biochem. Biophys. Res. Commun.*, **309**, 552–557.
Balint E, Bates S and Vousden KH. (1999). *Oncogene*, **18**, 3923–3929.
Carrano AC, Eytan E, Hershko A and Pagano M. (1999). *Nat. Cell Biol.*, **1**, 193–199.
Di Como CJ, Gaiddon C and Prives C. (1999). *Mol. Cell. Biol.*, **19**, 1438–1449.
Ganoth D, Bornstein G, Ko TK, Larsen B, Tyers M, Pagano M and Hershko A. (2001). *Nat. Cell Biol.*, **3**, 321–324.
Goldschneider D, Blanc E, Raguenez G, Barrois M, Legrand A, Le Roux G, Haddada H, Bebard J and Douc-Rasy S. (2004). *J. Cell Sci.*, **117**, 293–301.
Gong J, Costanzo A, Yang H-Q, Melino G, Kaelin WG, Levrero M and Wang JYJ. (1999). *Nature*, **399**, 806–809.
Ideguchi H, Ueda A, Tanaka M, Yang J, Tsuji T, Ohno S, Hagiwara E, Aoki A and Ishigatsubo Y. (2002). *Biochem. J.*, **367**, 87–95.
Jost C, Marin M and Kaelin WG. (1997). *Nature*, **389**, 191–194.
Kaghad M, Bonnet H, Yang A, Creancier L, Biscan JC, Valent A, Minty A, Chalon P, Lelias JM, Dumont X, Ferrara P, McKeon F and Caput D. (1997). *Cell*, **90**, 809–819.
Lee C-W and La Thangue NB. (1999). *Oncogene*, **18**, 4171–4181.
Li M, Chen D, Shiloh A, Luo J, Nikolaev AY, Qin J and Gu W. (2002). *Nature*, **416**, 648–653.
Lutz W, Frank EM, Craig TA, Thompson R, Venters RA, Kojetin D, Cavanagh J and Kumar R. (2003). *Biochem. Biophys. Res. Commun.*, **303**, 1186–1192.
Melino G, De Laurenzi V and Vousden KH. (2002). *Nat. Rev. Cancer*, **2**, 605–615.
Moll UM, Ostermeyer AG, Haladay R, Winkfield B, Frazier M and Zambetti G. (1996). *Mol. Cell. Biol.*, **16**, 1126–1137.
Nakagawa T, Takahashi M, Ozaki T, Watanabe K, Todo S, Mizuguchi H, Hayakawa T and Nakagawara A. (2002). *Mol. Cell. Biol.*, **22**, 2575–2585.
Nakamura M, Masuda H, Horii J, Kuma K, Yokoyama N, Ohba T, Nishitani H, Miyata T, Tanaka M and Nishimoto T. (1998). *J. Cell Biol.*, **143**, 1041–1052.
Nikolaev AY, Li M, Puskas N, Qin J and Gu W. (2003). *Cell*, **112**, 29–40.
Nishitani H, Hirose E, Uchimura Y, Nakamura N, Umeda M, Nishii K, Mori N and Nishimoto T. (2001). *Gene*, **272**, 25–33.
Ohtsuka T, Ryu H, Minamishima YA, Ryo A and Lee SW. (2003). *Oncogene*, **22**, 1678–1687.
Ozaki T, Watanabe K, Nakagawa T, Miyazaki K, Takahashi M and Nakagawara A. (2003). *Oncogene*, **22**, 3231–3242.
Ponting C, Schultz J and Bork P. (1997). *Trends Biochem. Sci.*, **22**, 193–194.
Pozniak CD, Radinovic S, Yang A, McKeon F, Kaplan DR and Miller FD. (2000). *Science*, **289**, 304–306.
Rao MA, Cheng H, Quayle AN, Nishitani H, Nelson CC and Rennie PS. (2002). *J. Biol. Chem.*, **277**, 48020–48027.
Ren J, Datta R, Shioya H, Li Y, Oki E, Biedermann V, Bharti A and Kufe D. (2002). *J. Biol. Chem.*, **277**, 33758–33765.
Stiewe T, Zimmermann S, Frilling A, Esche H and Putzer BM. (2002). *Cancer Res.*, **62**, 3598–3602.
Umeda M, Nishitani H and Nishimoto T. (2003). *Gene*, **303**, 47–54.
Wang D, Li Z, Messing EM and Wu G. (2002). *J. Biol. Chem.*, **277**, 36216–36222.
Wang Y, Schneider M, Li X, Duttenhofer I, Debatin K-M and Hug H. (2002). *Biochem. Biophys. Res. Commun.*, **297**, 148–153.
Watanabe K, Ozaki T, Nakagawa T, Miyazaki K, Takahashi M, Hosoda M, Hayashi S, Todo S and Nakagawara A. (2002). *J. Biol. Chem.*, **277**, 15113–15123.
Yuan Z-M, Shioya H, Ishiko T, Sun X, Gu J, Huang YY, Lu H, Kharbanda S, Weichselbaum R and Kufe D. (1999). *Nature*, **399**, 814–817.
Zeng X, Chen L, Jost CA, Maya R, Keller D, Wang X, Kaelin WG, Oren M, Chen J and Lu H. (1999). *Mol. Cell. Biol.*, **19**, 3257–3266.

Research Article

CpG Island Methylator Phenotype Is a Strong Determinant of Poor Prognosis in Neuroblastomas

Masanobu Abe,[1,2] Miki Ohira,[3] Atsushi Kaneda,[1] Yukiko Yagi,[1] Seiichiro Yamamoto,[4] Yoshihiro Kitano,[5] Tsuyoshi Takato,[2] Akira Nakagawara,[3] and Toshikazu Ushijima[1]

[1]Carcinogenesis Division, National Cancer Center Research Institute; [2]Department of Oral and Maxillo Facial Surgery, University of Tokyo Graduate School of Medicine; [3]Biochemistry Division, Chiba Cancer Center Research Institute; [4]Information Division, Research Center for Cancer Prevention and Screening, National Cancer Center; and [5]Department of Pediatric Surgery, National Center for Child Health and Development, Tokyo, Japan

Abstract

Neuroblastoma, one of the most common pediatric solid tumors, is characterized by two extreme disease courses, spontaneous regression and life-threatening progression. Here, we conducted a genome-wide search for differences in DNA methylation that distinguish between neuroblastomas of the two types. Three CpG islands (CGI) and two groups of CGIs were found to be methylated specifically in neuroblastomas with a poor prognosis. By quantitative analysis of 140 independent cases, methylation of all the five CGI (groups) was shown to be closely associated with each other, conforming to the CpG island methylator phenotype (CIMP) concept. The presence of CIMP was sensitively detected by methylation of the *PCDHB* CGIs and associated with significantly poor survival (hazard ratio, 22.1; 95% confidence interval, 5.3-93.4; $P < 0.0001$). Almost all cases with N-*myc* amplification (37 of 38 cases) exhibited CIMP. Even in 102 cases without N-*myc* amplification, the presence of CIMP (30 cases) strongly predicted poor survival (hazard ratio, 12.4; 95% confidence interval, 2.6-58.9; $P = 0.002$). Methylation of *PCDHB* CGIs, located in their gene bodies, did not suppress gene expression or induce histone modifications. However, CIMP was significantly associated with methylation of promoter CGIs of the *RASSF1A* and *BLU* tumor suppressor genes. The results showed that neuroblastomas with CIMP have a poor prognosis and suggested induction of silencing of important genes as an underlying mechanism. (Cancer Res 2005; 65(3): 828-34)

Introduction

Epigenetic abnormalities, especially alterations in DNA methylation, are intimately involved in development of various human tumors (1). Aberrant methylation of promoter CpG islands (CGI) causes inactivation of tumor suppressor genes. Genomic instability is caused by genomic hypomethylation and is associated with hypermethylation (2, 3). Identification of epigenetic abnormalities in human cancers is expected to lead not only to discovery of novel disease mechanisms but also to development of new diagnostic markers. Therefore, we previously developed a genome-wide scanning method, methylation-sensitive representational difference analysis (MS-RDA), for detecting differences in DNA methylation (4, 5). This technique analyzes unmethylated, CpG-rich regions of the genome and has already identified genes silenced in human lung, stomach, breast, and pancreatic cancers (6–9).

Neuroblastoma derived from primitive cells of the sympathetic nervous system is one of the most common solid tumors in childhood, characterized by two extreme disease courses, spontaneous regression, and life-threatening progression (10, 11). The clinical outcome is associated with disease stage, age at diagnosis, histologic classification, N-*myc* amplification, DNA ploidy, and *TrkA* overexpression (10–12). These characteristics are therefore used to classify cases into low-, intermediate-, and high-risk groups. However, especially in the cases with intermediate risk, prediction of prognosis and therapeutic decision-making are still difficult, and development of new markers is an urgent priority. Moreover, the molecular bases underlying the two distinct clinical courses are still unknown, and their clarification is needed to allow development of novel therapeutics.

In the present study, considering the major involvement of epigenetic machinery in embryonic development (13, 14), we searched for differences in DNA methylation between neuroblastomas with a good prognosis and counterparts with a poor prognosis by MS-RDA.

Materials and Methods

Tissue Samples and Cell Lines. Tumor samples were obtained from 145 nonrecurrent cases between 1995 and 1999 and were used under approval of institutional review boards. The mean age at initial diagnosis was 27 months (range, 0-216 months). Their clinical stages were determined according to the International Neuroblastoma Staging System, and 40, 17, 20, 60, and 8 cases belonged to stages I, II, III, IV, and IVS, respectively. Normal adrenal medulla tissue was collected from a case undergoing nephrectomy for a renal cancer. Neuroblastoma cell lines were obtained from the American Type Culture Collection (Manassas, VA), the Japanese Collection of Research Bioresources (Tokyo, Japan), and the RIKEN Bio Resource Center (Tsukuba, Japan). GANB was established by A.N. and normal human bronchial epithelial cells were purchased from Cambrex (East Rutherford, NJ). High molecular weight DNA and total RNA were extracted as previously described (7). Total RNAs of brain and adrenal glands were purchased from Clontech (Palo Alto, CA).

MS-RDA and Database Search. MS-RDA was done as previously described (4, 5). Genomic DNA of primary neuroblastomas with a good prognosis (cases 92, 98, 104, 112, and 148) and neuroblastoma cell lines established from cases with a poor prognosis (CHP134, IMR32, GANB, NGP, and TGW) were digested with *Hpa*II, and then two pooled DNA samples were prepared. Although use of cell lines is highly recommended for MS-RDA (5), no cell lines were available for neuroblastomas with a good prognosis, and therefore we used the primary samples. To isolate CGIs that were hypermethylated in the latter, the cell line pool was used as the tester, and the primary tumor pool as the driver. MS-RDA in the opposite direction

Note: Supplementary data for this article are available at Cancer Research online (http://cancerres.aacrjournals.org/).

Requests for reprints: Toshikazu Ushijima, 5-1-1 Tsukiji, Chuo-ku, Tokyo 104-0045, Japan. Phone: 133-547-5240; Fax: 135-565-1753; E-mail: tushijim@ncc.go.jp.

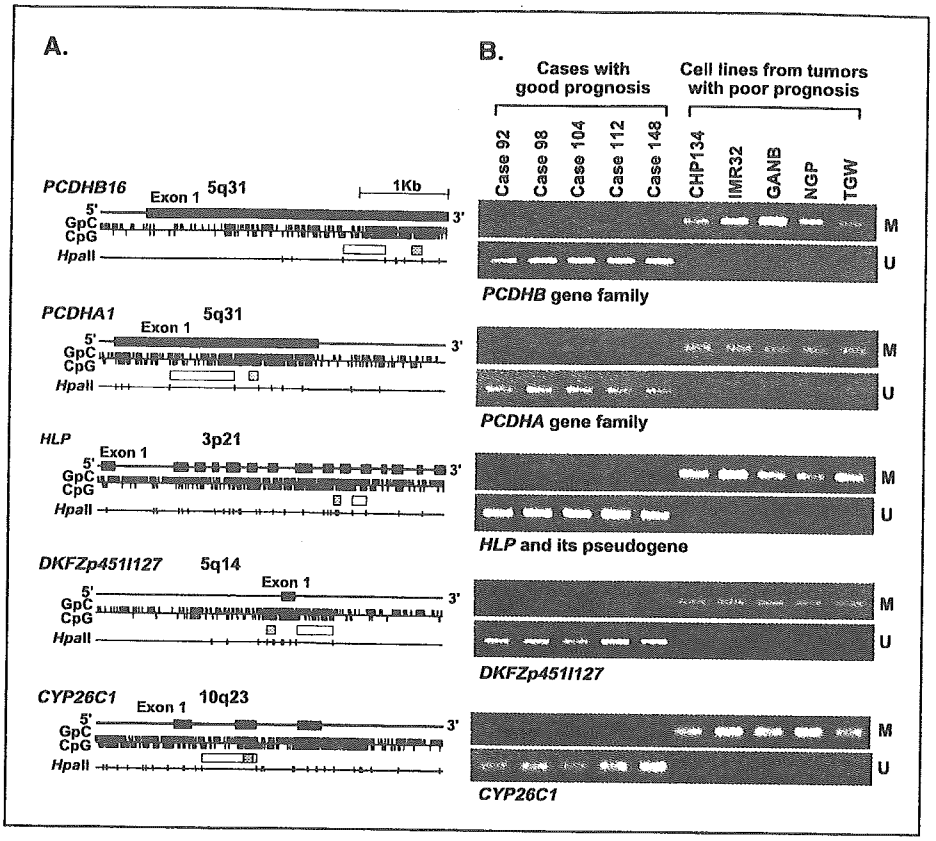

Figure 1. Five CGIs isolated by MS-RDA and their methylation statuses in the samples used for MS-RDA. *A*, genomic structures of the five CGIs. GpC, CpG, and *Hpa*II recognition sites (5′-CCGG-3′) are shown by ticks. *Closed boxes*, exons; *open boxes*, clones isolated by MS-RDA; *shaded boxes*, regions analyzed by MSP. *B*, methylation statuses analyzed by MSP. *M*, MSP using primers specific to methylated DNA; *U*, MSP using primers specific to unmethylated DNA. All the five CGIs were found to be differentially methylated between the two groups used for MS-RDA.

was also done. For each series of MS-RDA, 96 clones were analyzed for redundancy, and nonredundant clones were sequenced. Their genomic origins were examined using BLASTN software http://www.ncbi.nlm.nih.gov/BLAST/).

Sodium Bisulfite Modification and Methylation-Specific PCR. One microgram of DNA underwent sodtlbium bisulfite modification (15), and was suspended in 20 μL of TE buffer. For methylation-specific PCR (MSP), 1 μL of the solution was used for PCR with primers specific to methylated or unmethylated sequences. Using DNA from normal human bronchial epithelial and DNA methylated with *Sss*I methylase, annealing temperatures specific for methylated and unmethylated primers were determined. Quantitative MSP was done separately for methylated DNA molecules and for unmethylated DNA molecules. Standard DNA was prepared by cloning PCR products amplified by methylated and unmethylated primers into a vector, respectively. The numbers of methylated and unmethylated molecules in a test sample were determined by comparing their amplification with those of standard samples containing 10 to 10^6 molecules. The "methylation index" was calculated as the fraction of methylated molecules in the total DNA molecules (no. methylated molecules + no. unmethylated molecules). Each sample was analyzed twice, blind to clinical information, and high reproducibility was confirmed (correlation coefficient = 0.98).

The *protocadherin* β (*PCDHB*) family consists of 16 genes with single exons and three pseudogenes on 5q31, and their CGIs are located in the gene bodies. MSP primers were designed to recognize 17 of the 19 members (all except for the *PCDHB1* gene and the *PCDHB19* pseudogene). The *protocadherin* α (*PCDHA*) family consists of 15 genes and one pseudogene having unique first exons and shared exons 2 to 4 on 5q31, and their CGIs are located in exon 1. MSP primers were designed to recognize 13 of the 16 members (all except for the *PCDHAC1* and *PCDHAC2* genes and the *PCDHA14* pseudogene). The *hepatocyte growth factor-like protein* (*HLP/MSP/MST1*) gene is highly homologous to *macrophage stimulating, pseudogene 9* (*MSTP9*), and MSP primers were designed to recognize both of these. For *DKFZp451I127*, *FLJ37440*, *Zinc finger protein 297* (*ZNF297*), and *Cytochrome p450 CYP26C1* (*CYP26C1*), MSP primers were designed to recognize each of them specifically. The primers and PCR conditions are shown in Supplementary Table 1.

Semiquantitative and Quantitative Reverse Transcription-PCR. cDNA was synthesized from 3 μg of total RNA treated with DNase using a Superscript II kit (Invitrogen Co., Carlsbad, CA). For semiquantitative reverse transcription-PCR (*PCDHB1-PCDHB15*), multiple cycles of PCR were tested for each gene, and numbers giving a wide dynamic range were determined. The primers and PCR conditions are shown in Supplementary Table 2. For quantitative reverse transcription-PCR (*PCDHB16*), the number of cDNA molecules was determined by quantitative PCR, as in quantitative MSP, and the copy number was normalized to that of *GAPDH*.

Chromatin Immunoprecipitation Assay. From 1×10^6 cells, DNA/histone complexes were immunoprecipitated, and DNA was eluted in 30 μL of TE after reversing cross-linking. Copy numbers of DNA molecules of the *PCDHB16* exon, *RASSF1A* promoter, and *GAPDH* promoter in 1 L of the eluate were determined by quantitative PCR (primer sequences in Supplementary Table 3), and normalized to the copy numbers in the input. Anti-acetyl-histone H3 antibody (AcH3) and anti-dimethylated-histone H3 (lysine 9; MetH3K9) were purchased from Cell Signalling (Beverly, MA).

Statistical Analysis. Associations between methylation levels among CGI groups were examined using the Pearson correlation coefficient and Fisher's exact test. Survival time was measured from the date of initial diagnosis to the date of death or last contact. Kaplan-Meier analysis and log-rank tests were done to compare survival between the groups defined by methylation levels. Hazard ratio (HR) between groups and dose-response relationships between methylation levels and survival were estimated by the Cox proportional hazard model. Kaplan-Meier curves were drawn with the help of Aabel software (Gigawiz. Ltd. Co., Tulsa, OK) and other analyses were conducted using SAS version 8.2 (SAS Institute, Inc., Cary, NC).

Results

Genome-Scanning for Differentially Methylated CpG Islands. MS-RDA was done using five primary neuroblastomas with a good prognosis and five neuroblastoma cell lines established from cases with a poor prognosis. Seven DNA fragments, derived from CGIs of *PCDHB16*, *PCDHA1*, *HLP*, *DKFZp451I127*, *FLJ37440*, *ZNF297*, and *CYP26C1*, were isolated as methylated in the latter samples. No DNA fragments were isolated as methylated in the former samples. Methylation statuses of (i) 17 CGIs of the *PCDHB* family (detailed structure in Supplementary Fig. 1), (ii) 13 CGIs of the *PCDHA* family, (iii) *HLP* and its pseudogene, and (iv) other four unique CGIs were examined by MSP. This revealed that the *PCDHB* family (5q31), the *PCDHA* family (5q31), *HLP* (3p21) and its pseudogene (1p36), *DKFZp451I127* (5q14), and *CYP26C1* (10q23) were specifically methylated in the latter samples (Fig. 1*A* and *B*).

Close Association between Methylation and Poor Prognosis in 140 Independent Primary Samples. To analyze the significance of the differential methylation of the above five CGI (groups) in primary neuroblastomas, 140 primary samples, all different from the initial five samples, were analyzed by quantitative MSP. When distributions of methylation indices were analyzed (Fig. 2), a clear bimodal distribution was observed for (i) the CGI group in the *PCDHB* family (17 CGIs), (ii) the CGIs of *HLP* and its pseudogene, and (iii) the *CYP26C1* CGI. The results thus indicated that the cases could be classified into two groups, one with high methylation and the other with low methylation. The dose-response relationships between high *PCDHB* methylation and poor prognosis were analyzed by the Cox proportional model using the methylation index as a continuous value, and the association was confirmed with a trend $P < 0.0001$. Normal adrenal medulla had a methylation index of 4%.

According to the bimodal distribution, the effect of high methylation was assessed by dichotomous groups. For the *PCDHB* family, cutoff values of 30%, 40%, 50%, 60%, 70%, and 80% were tested, and HRs of 16.8 [95% confidence interval (95% CI), 4.0-70.9], 22.1 (95% CI, 5.3-93.4; Fig. 3), 13.1 (95% CI, 4.5-37.9), 9.1 (95% CI, 3.8-23.4), 7.0 (95% CI, 3.1-15.8), and 7.8 (95% CI, 3.4-17.6), respectively, were obtained ($P < 0.001$ for all cutoff values). This showed that cases can be classified into two groups with distinct prognoses, and we adopted a cutoff value of 40%, which gave the highest HR, for convenience in the following analysis.

The dose-response relationships were also confirmed for other four CGI (groups), *PCDHA* ($P = 0.004$), *HLP* ($P < 0.0001$), *DKFZp451I127* ($P = 0.02$), and *CYP26C1* ($P < 0.0001$). Cutoff values were similarly tested, and those for *PCDHA*, *HLP*, *DKFZp451I127*, and *CYP26C1* were set at 80%, 10%, 20%, and 70%, respectively, with HRs of 5.7 (95%CI, 1.4-24.0; $P = 0.07$), 21.7 (95% CI, 5.1-91.4; $P < 0.0001$), 3.2 (95% CI, 1.0-10.5; $P = 0.045$), and 8.7 (95% CI, 4.1-18.1; $P < 0.0001$), respectively (Fig. 3).

Existence of the CpG Island Methylator Phenotype in Neuroblastomas. Methylation of the different CGI (groups) had shown close associations with each other (Table 1). When correlation was analyzed as a continuous value, Pearson correlation coefficients between *PCDHB* and *PCDHA*, *HLP*, *DKFZp451I127* and *CYP26C1* were 0.55, 0.70, 0.26 and 0.77, respectively. This showed that multiple CGIs were simultaneously methylated in

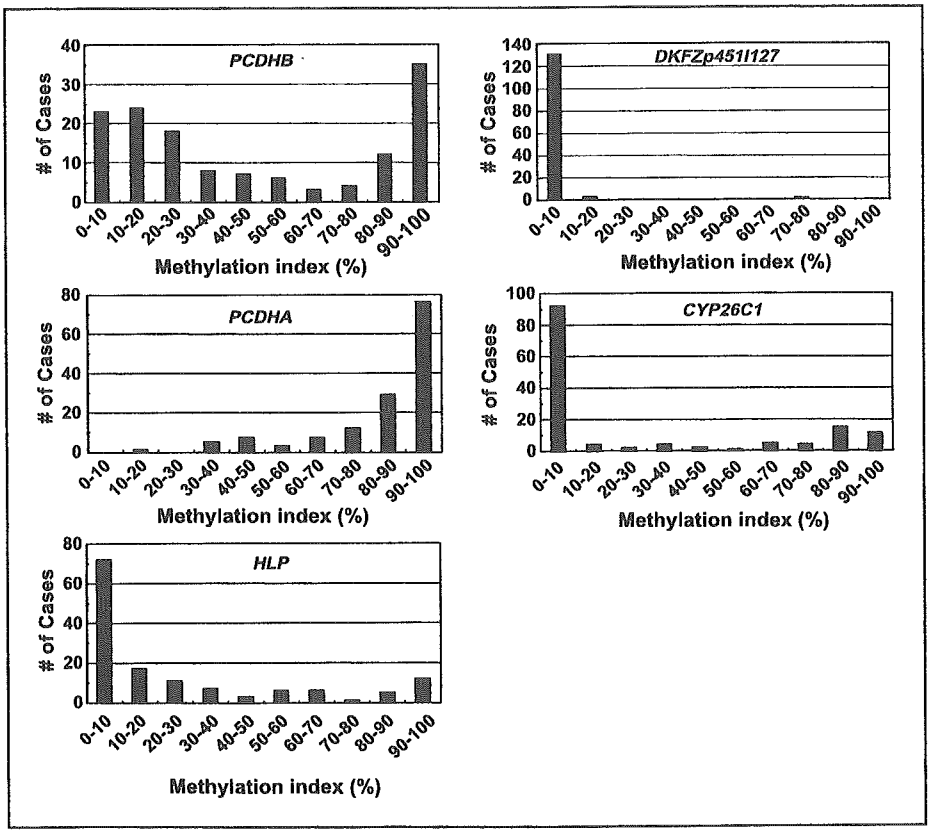

Figure 2. The distribution of methylation indices among the 140 cases analyzed: (*i*) 17 CGIs of the *PCDHB* family, (*ii*) 13 CGIs of the *PCDHA* family, (*iii*) CGIs of *HLP* and its pseudogene, (*iv*) *DKFZp451I127*, and (*v*) *CYP26C1*.

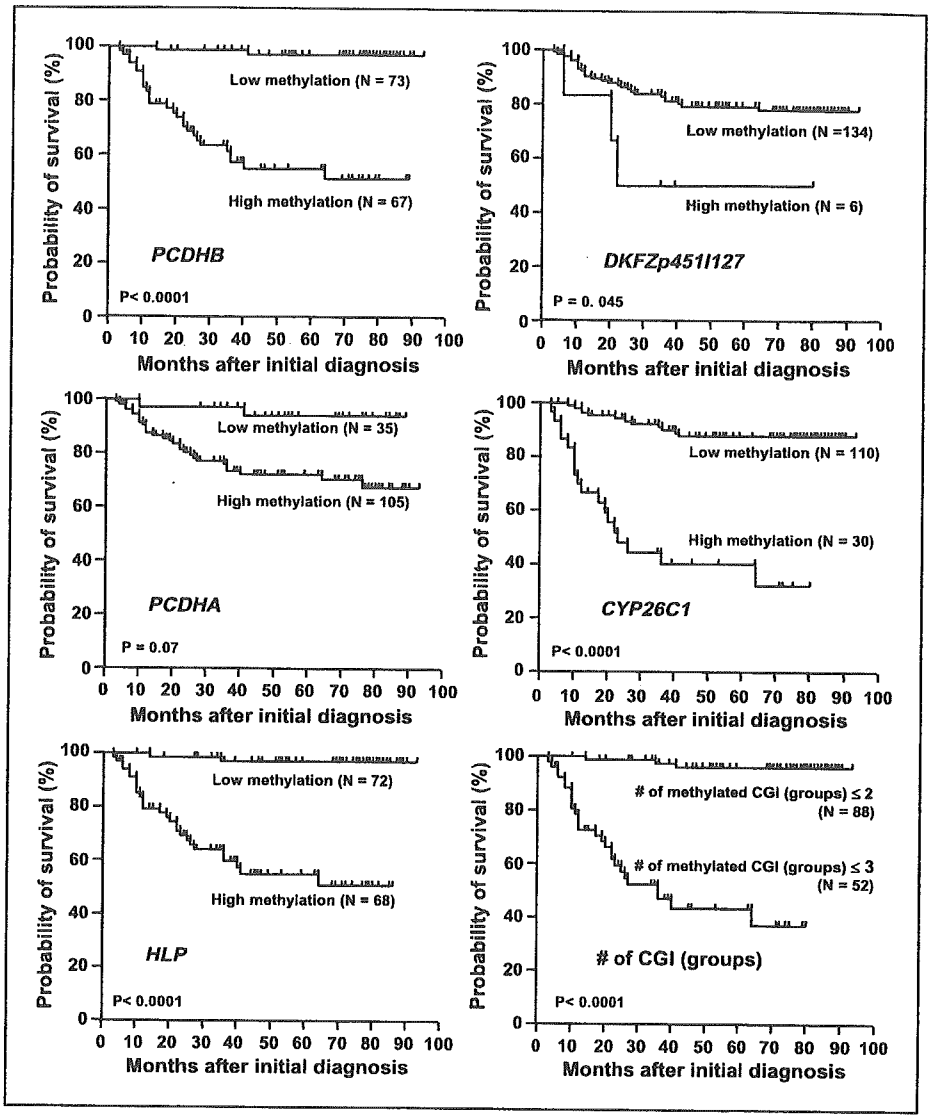

Figure 3. Predictive powers of methylation of the five CGI (groups) identified, and their multiple methylation: (*i*) 17 CGIs of the *PCDHB* family, (*ii*) 13 CGIs of the *PCDHA* family, (*iii*) CGIs of *HLP* and its pseudogene, (*iv*) *DKFZp451I127*, (*v*) *CYP26C1*, and (*vi*) methylation of three of these or more were analyzed by the Kaplan-Meier method using 140 primary samples. The *PCDHB* family, *HLP*, *DKFZp451I127*, *CYP26C1*, and methylation of multiple CGI (groups) had significant influence on survival.

neuroblastomas with a poor prognosis (Supplementary Fig. 2*A*). The simultaneous methylation of (i) 17 CGIs of the *PCDHB* family, (ii) 13 CGIs of the *PCDHA* family, (iii) CGIs of *HLP* and its pseudogene, (iv) *DKFZp451I127* CGI, and (v) *CYP26C1* CGI conformed with the concept of the CpG island methylator phenotype (CIMP; ref. 16).

Associations between CIMP and poor prognosis were examined by defining CIMP as cases with methylation of two CGI (groups) or more, those with three or more, those with four or five, and those with five. When CIMP was defined as cases with methylation of three CGI (groups) or more, the largest association with poor prognosis was observed, with a HR of 25.4 (95% CI, 7.6-84.5; Fig. 3). However, the HR (22.1) given by 17 CGIs of the *PCDHB* gene family approximated to this, and the *PCDHB* methylation level closely correlated with the number of methylated CGI (groups; Supplementary Fig. 2*B*). Therefore, for simplicity of analysis, we defined CIMP in neuroblastomas on the basis of high methylation of the *PCDHB* family, tentatively with a cutoff value of 40%.

Predictive Power of CIMP, Compared with Known Prognostic Factors. Univariate analyses showed that N-*myc* amplification, low *TrkA* expression, DNA diploidy, and an age no younger than 1 year gave HRs of 9.5 (95% CI, 4.4-20.5), 3.9 (95% CI, 1.7-9.3), 4.2 (95% CI, 1.65-10.8), and 12.3 (95% CI, 3.7-41.7). Cases were stratified by these known factors (Table 2). In those without N-*myc* amplification, CIMP also showed an influence with a HR of 12.4 (95% CI, 2.6-58.9), but almost all cases with N-*myc* amplification (37 of the 38 cases) showed CIMP. It was suggested that cases with N-*myc* amplification were contained in the cases with CIMP. CIMP was independent from *TrkA* overexpression, DNA ploidy, and age at diagnosis. Stage seemed to be a stronger prognostic factor. Notably, even when limited to cases in stages III and IV without N-*myc* amplification, which are classified into the intermediate risk group and clinically important, CIMP gave a HR of 4.8 (95% CI, 1.0-23.0; $P = 0.048$).

Multivariate analyses were finally done taking all the five known prognostic factors into account. Although CIMP gave a HR of 5.0 (95% CI, 0.47-52.7), it was not significant ($P = 0.18$), possibly due to limitation in the number of cases.

Table 1. Association between the *PCDHB* methylation and methylation of other CGIs

Variables	Methylation level of *PCDHB* family gene		*P**
	High (≥40%)	Low (<40%)	
No. cases (n = 140)	67	73	
Methylation of CGIs outside promoter regions (n = 140)			
PCDHA gene family (exon 1)†	65/67	41/73	<0.0001
HLP (exons 2-13)‡	52/67	16/73	<0.0001
CYP26C1 (exon 2)§	30/67	0/73	<0.0001
p41Arc (intron 8)	1/67	1/73	0.48
SIM2 (exon 2)	0/67	0/73	
Methylation of CGIs in promoter regions (n = 140)			
DKFZp451I127‖	6/67	0/73	0.011
RASSF1A	51/67	10/73	<0.0001
BLU	25/67	3/73	<0.0001
p16	0/67	0/73	
hMLH1	0/67	0/73	
PCDHB1	0/67	0/73	
TAF7	0/67	0/73	
p41Arc	0/67	0/73	
SIM2	0/67	0/73	

*Fisher's exact test.
†Boundaries for high methylation and low methylation of *PCDHA* gene family were set at 80% of the methylation index.
‡Boundaries for high methylation and low methylation of *HLP* were set at 10% of the methylation index.
§Boundaries for high methylation and low methylation of *CYP26C1* were set at 70% of the methylation index.
‖Boundaries for high methylation and low methylation of *DKFZp451I127* were set at 20% of the methylation index.

Effects of PCDHB Methylation on Gene Expression and Chromatin Structure. The CGIs of the *PCDHB* family were located in their gene bodies, whose methylation generally does not block gene transcription (17). The actual effects of methylation on expression were examined for 16 genes of the *PCDHB* family using 10 primary neuroblastomas with low methylation and five primary neuroblastomas with high methylation. The methylation was not associated with loss of expression (a representative result is shown in Fig. 4*A*). The effect of methylation of the *PCDHB16* CGI on the histone modification was further examined by chromatin immunoprecipitation assay. It was found that DNA methylation of the *PCDHB16* CGI did not induce histone H3 lysine 9 methylation or histone H3 deacetylation (data not shown).

Association between CIMP and Promoter Methylation. High methylation of *PCDHB* CGIs, a sensitive surrogate marker of CIMP in neuroblastomas, did not repress gene expression or induce histone modification. This indicated that CIMP is involved in the poor prognosis of neuroblastomas by causing methylation of promoter CGIs, although it is known that promoter CGIs are resistant to *de novo* methylation (18, 19).

Among the five CGI (groups) identified in this study, only that of *DKFZp451I127* was located in a promoter region. Although its methylation was infrequent, the methylation was observed only in neuroblastomas with CIMP (Table 1), and was associated with expression loss (Fig. 4*B*). To make the association clearer, methylation statuses were analyzed for eight additional CGIs in promoter regions. It was shown that methylation of promoter CGIs of *RASSF1A* (3p21) and *BLU* (3p21) was far more frequently observed in neuroblastomas with CIMP (Table 1, $P < 0.0001$). At the same time, there was a preference for CGIs affected by CIMP among CGIs in promoter regions, and also among those outside promoter regions (Table 2).

Discussion

Extensive methylation of multiple CGIs, conforming with the concept of CIMP, was here found specifically present in neuroblastomas with a poor prognosis and could be sensitively detected by focusing on the *PCDHB* family. *PCDHB* methylation did not suppress gene expression or induce histone modification. However, CIMP was associated with promoter methylation of *RASSF1A* and *BLU* genes and one of the mechanisms underlying the poor prognosis of neuroblastomas seemed to be silencing of these and possibly other tumor suppressor genes and genes important for differentiation.

CIMP was originally identified in colon cancers (16), but there has been some dispute over its presence (20). The clear correlation between CIMP and a poor prognosis found here for neuroblastomas was unequivocal and presumably reflects an intrinsic tendency for methylation of CGIs. This is because, first, neuroblastomas have a much shorter history than colon cancers, and the accumulated number of methylated CGIs in neuroblastomas is expected to parallel the speed of occurrence of

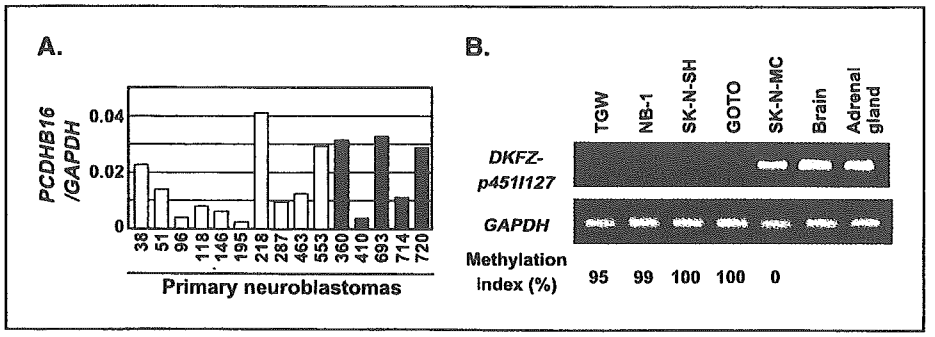

Figure 4. Effects of methylation of the *PCDHB* family and *DKFZp451I127* on gene expression. *A*, *PCDHB16* expression was analyzed by quantitative RT-PCR in 10 primary samples with low methylation (*open columns*) and five primary samples with high methylation (*closed columns*), and no difference was observed between the two groups. *B*, silencing of *DKFZp451I127* by methylation of its promoter CGI. The CGI was methylated in four cell lines, TGW, NB-1, SK-N-SH, and GOTO, whereas it was unmethylated in one cell line, SK-N-MC. *DKFZp451I127* was expressed in SK-N-MC, but not expressed at all in the four cell lines with the promoter methylation.

Table 2. HRs of death by *PCDHB* methylation status in subgroup of known prognostic factors

Stratified by		*PCDHB* methylation	No. cases	No. deaths	HR* (95% CI)	*P*†
Overall (n = 140)		High	67	1	22.1 (5.3-93.4)	< 0.0001
		Low	73	2	1	
N-*myc* amplification (n = 140)	No	High	30	8	12.4 (2.6-58.9)	0.002
		Low	72	2	1	
	Yes	High	37	20	NE	—
		Low	1	0		
TrkA overexpression (n = 130)	Yes	High	20	6	18.3 (2.2-152.6)	0.007
		Low	49	1	1	
	No	High	40	19	NE	
		Low	21	0		
DNA ploidy (n = 125)	Aneuploid	High	17	5	18.3 (2.1-156.7)	0.008
		Low	49	1	1	
	Diploid	High	38	17	NE	
		Low	21	0		
Clinical stages (n = 140)	Stages I, II, and IVS	High	8	0	NE	—
		Low	52	0		
	Stages III and IV	High	59	28	7.4 (1.8-31.3)	0.006
		Low	21	2	1	
Age at diagnosis (n = 140)	<1	High	11	3	NE	
	≥1	Low	59	0		
		High	56	25	4.5 (1.1-18.9)	0.043
		Low	14	2	1	

*HR of death for a case with high *PCDHB* methylation compared with a case with low methylation. NE shows not estimable due to no events in at least one category.
†Significance level for a high *PCDHB* methylation to low methylation using Cox proporitonal model.

methylation. Second, methylation of the *PCDHB* family did not affect gene expression, and there should have been no selection of cells with the *PCDHB* methylation, in contrast to the case of promoter methylation of tumor suppressor genes. Investigation into the mechanism of the intrinsic tendency for methylation of multiple CGIs is necessary. Furthermore, alleviation of the intrinsic tendency could block progression of neuroblastomas and have potential therapeutic value.

Among the six CGI (groups) outside promoter regions analyzed here, CIMP in neuroblastomas preferentially affected four CGI (groups); those of the *PCDHB* family, the *PCDHA* family, *HLP*, and *CYP26C1*. Unexpectedly, three CGIs that are known to be frequently methylated in human colon cancers with CIMP, MINT1, MINT2, and MINT17 (16) were not methylated in neuroblastoma cell lines (data not shown). Among the nine CGIs in promoter regions analyzed, CIMP in neuroblastomas affected only three, those of *RASSF1A*, *BLU*, and *DKFZp451I127*. The nine CGIs were selected based upon previous reports as tumor suppressor genes (*RASSF1A*, *BLU*, *p16*, and *hMLH1*; refs. 21–23), the chromosomal location flanking the *PCDHB* family (*PCDHB1* and *TAF7*), our previous report on the fidelity in inheriting methylation patterns (*p41Arc* and *SIM2*; ref. 19), and the findings here (*DKFZp451I127*). Because gene expression and possibly chromatin structures affect the frequency of *de novo* methylation (24, 25), the available data suggest that CGIs useful to sensitively detect CIMP might vary according to the tumor type.

The influence of CIMP on prognosis was here found to be comparable to that of the currently most reliable marker, N-*myc* amplification, and stronger than *TrkA* overexpression and DNA ploidy on univariate analysis. Subgroup analysis showed that the influence was independent of *TrkA* overexpression, DNA ploidy and age at diagnosis and CIMP had influence even in cases without N-*myc* amplification and in advanced stages. These points strongly indicated CIMP to be a promising new prognostic marker. However, the cutoff values adopted here are tentative, and the HRs obtained could have been overestimated. A validation study using independent samples is necessary for further evaluation. The fact that cases with CIMP contained almost all the cases with N-*myc* amplification suggested that a common molecular mechanism caused both alterations, or that CIMP may lead to N-*myc*

amplification. Whatever the case, the findings might provide clues to molecular mechanisms of neuroblastoma development.

In summary, the present study showed that CIMP is present specifically in neuroblastomas with poor prognosis and that can be sensitively detected by focusing on *PCDHB* methylation. CIMP seems to be a promising new prognostic marker, and its evaluation and investigations into the mechanisms underlying CIMP in neuroblastomas seem warranted.

Acknowledgments

Received 7/27/2004; revised 11/14/2004; accepted 11/24/2004.

Grant support: Grant-in-aid for the Third-term Cancer Control Strategy Program from the Ministry of Health, Labour, and Welfare, Japan and Research Resident Fellowship from the Foundation for Promotion of Cancer Research (M. Abe).

The costs of publication of this article were defrayed in part by the payment of page charges. This article must therefore be hereby marked advertisement in accordance with 18 U.S.C. Section 1734 solely to indicate this fact.

We thank Drs. E. Okochi-Takada and G. S. Goldberg for critical reading of the article and the institutions for participation in the collection of clinical materials.

References

1. Jones PA, Baylin SB. The fundamental role of epigenetic events in cancer. Nat Rev Genet 2002;3:415–28.
2. Chen RZ, Pettersson U, Beard C, Jackson-Grusby L, Jaenisch R. DNA hypomethylation leads to elevated mutation rates. Nature 1998;395:89–93.
3. Kondo Y, Kanai Y, Sakamoto M, et al. Genetic instability and aberrant DNA methylation in chronic hepatitis and cirrhosis-A comprehensive study of loss of heterozygosity and microsatellite instability at 39 loci and DNA hypermethylation on 8 CpG islands in microdissected specimens from patients with hepatocellular carcinoma. Hepatology 2000;32:970–9.
4. Ushijima T, Morimura K, Hosoya Y, et al. Establishment of methylation-sensitive-representational difference analysis and isolation of hypo- and hypermethylated genomic fragments in mouse liver tumors. Proc Natl Acad Sci U S A 1997;94:2284–9.
5. Kaneda A, Takai D, Kaminishi M, Okochi E, Ushijima T. Methylation-sensitive representational difference analysis and its application to cancer research. Ann N Y Acad Sci 2003;983:131–41.
6. Takai D, Yagi Y, Wakazono K, et al. Silencing of *HTR1B* and reduced expression of *EDN1* in human lung cancers, revealed by methylation-sensitive representational difference analysis. Oncogene 2001; 20:7505–13.
7. Kaneda A, Kaminishi M, Yanagihara K, Sugimura T, Ushijima T. Identification of silencing of nine genes in human gastric cancers. Cancer Res 2002;62:6645–50.
8. Miyamoto K, Asada K, Fukutomi T, et al. Methylation-associated silencing of heparan sulfate *D-glucosaminyl 3-O-sulfotransferase-2* (*3-OST-2*) in human breast, colon, lung and pancreatic cancers. Oncogene 2003;22:274–80.
9. Hagihara A, Miyamoto K, Furuta J, et al. Identification of 27 5′ CpG islands aberrantly methylated and 13 genes silenced in human pancreatic cancers. Oncogene 2004;23:8705–10.
10. Brodeur GM. Neuroblastoma: biological insights into a clinical enigma. Nat Rev. Cancer 2003;3:203–16.
11. Schwab M, Westermann F, Hero B, Berthold F. Neuroblastoma: biology and molecular and chromosomal pathology. Lancet Oncol 2003;4:472–80.
12. Nakagawara A, Arima-Nakagawara M, Scavarda NJ, et al. Association between high levels of expression of the *TRK* gene and favorable outcome in human neuroblastoma. N Engl J Med 1993;328:847–54.
13. Jaenisch R, Bird A. Epigenetic regulation of gene expression: how the genome integrates intrinsic and environmental signals. Nat Genet 2003;33:245–54.
14. Li E. Chromatin modification and epigenetic reprogramming in mammalian development. Nat Rev Genet 2002;3:662–73.
15. Kaneda A, Kaminishi M, Sugimura T, Ushijima T. Decreased expression of the seven ARP2/3 complex genes in human gastric cancers. Cancer Lett 2004; 212:203–10.
16. Toyota M, Ahuja N, Ohe-Toyota M, et al. CpG island methylator phenotype in colorectal cancer. Proc Natl Acad Sci U S A 1999;96:8681–6.
17. Gonzalgo ML, Hayashida T, Bender CM, et al. The role of DNA methylation in expression of the *p19/p16* locus in human bladder cancer cell lines. Cancer Res 1998;58:1245–52.
18. Nguyen C, Liang G, Nguyen TT, et al. Susceptibility of nonpromoter CpG islands to *de novo* methylation in normal and neoplastic cells. J Natl Cancer Inst 2001; 93:1465–72.
19. Ushijima T, Watanabe N, Okochi E, et al. Fidelity of the methylation pattern and its variation in the genome. Genome Res 2003;13:868–74.
20. Yamashita K, Dai T, Dai Y, Yamamoto F, Perucho M. Genetics supersedes epigenetics in colon cancer phenotype. Cancer Cell 2003;4:121–31.
21. Agathanggelou A, Dallol A, Zochbauer-Muller S, et al. Epigenetic inactivation of the candidate 3p21.3 suppressor gene *BLU* in human cancers. Oncogene 2003; 22:1580–8.
22. Takita J, Hayashi Y, Nakajima T, et al. The *p16* (*CDKN2A*) gene is involved in the growth of neuroblastoma cells and its expression is associated with prognosis of neuroblastoma patients. Oncogene 1998; 17:3137–43.
23. Harada K, Toyooka S, Maitra A, et al. Aberrant promoter methylation and silencing of the *RASSF1A* gene in pediatric tumors and cell lines. Oncogene 2002; 21:4345–9.
24. De Smet C, Loriot A, Boon T. Promoter-dependent mechanism leading to selective hypomethylation within the 5′ region of gene *MAGE-A1* in tumor cells. Mol Cell Biol 2004;24:4781–90.
25. Richards EJ, Elgin SC. Epigenetic codes for heterochromatin formation and silencing: rounding up the usual suspects. Cell 2002;108:489–500.

Available online at www.sciencedirect.com
SCIENCE DIRECT®
Cancer Letters 228 (2005) 5–11
CANCER Letters
www.elsevier.com/locate/canlet

Mini-review

A review of DNA microarray analysis of human neuroblastomas

Miki Ohira[a], Shigeyuki Oba[b], Yoko Nakamura[a], Takahiro Hirata[c], Shin Ishii[b], Akira Nakagawara[a,*]

[a]*Division of Biochemistry, Chiba Cancer Center Research Institute, 666-2 Nitona, Chuoh-ku, Chiba 260-8717, Japan*
[b]*Graduate School of Information Science, Nara Institute of Science and Technology, Ikoma 630-0192, Japan*
[c]*Hisamitsu Pharmaceutical Co. Inc., Tokyo 100-622, Japan*

Received 20 December 2004; accepted 12 January 2005

Abstract

Neuroblastoma (NBL) is an enigmatic tumor with heterogeneous clinical behaviors including maturation, regression, and aggressive growth. Despite recent progress in therapeutic strategies against advanced NBL, long-term outcomes still remain very poor. The prediction of cancer prognosis is one of the most urgent demands to initiate the suitable treatment of NBL. Recent papers have demonstrated that cancers can be diagnosed on the basis of gene expression profiling. We have been proceeded NBL cDNA project to collect a large number of genes expressed in NBLs, to identify the genes differentially expressed between favorable and unfavorable NBLs, and to make an NBL-proper cDNA chip for large-scale analysis of NBL tumors. Computational analysis of gene expression data in NBLs identified many prognosis-related genes and provided a classifier to predict the patient prognosis with high efficiency. Conversion of these findings into better diagnosis and treatment is now underway. Thus, molecular profiling of NBL has become a feasible tool for clinical applications.

Keywords: Neuroblastoma; Expression profile; Microarray; Diagnosis; Prognosis prediction; Differential expression

1. Introduction

Neuroblastoma (NBL) is one of the most frequent solid cancers in young children and has variable clinical and biological characteristics [1]. Favorable type of tumors frequently regress spontaneously, while unfavorable type of tumors are often resistant to intensive chemotherapy and lead patients to fatal outcome. The poor prognosis of NBL patients depends on age at diagnosis (older than 12 months), advanced tumor stage (3 or 4), presence of *MYCN* amplification, low *TRKA* expression, unfavorable histology, diploidy, and chromosomal loss of 1p36 in tumors [2]. However, even these markers sometimes fail to classify the aggressiveness of tumors, especially for the intermediate type of NBL (stage 3 or 4 patients with single copy of *MYCN*). Moreover, some *MYCN*-amplified tumors can be distinguished by a better response to the combined treatment resulting in a better prognosis for

* Corresponding author. Tel.: +81 43 264 5431; fax: +81 43 265 4459.
E-mail address: akiranak@chiba-cc.jp (A. Nakagawara).

0304-3835/$ - see front matter © 2005 Elsevier Ireland Ltd. All rights reserved.
doi:10.1016/j.canlet.2005.01.054

Table 1
Genes whose expression is differential between neuroblastoma subsets and related to patient prognosis

Genes	Definition	Pattern[a]	Reference
TRKA	neurotrophic tyrosine kinase, receptor, type 1	F>UF	[3]
CD44	CD44 antigen	F>UF	[6]
PTN	Pleiotrophin	F>UF	[7]
CDC10	cell division cycle 10	F>UF	[10]
HRAS	v-Ha-ras Harvey rat sarcoma viral oncogene	F>UF	[9]
XCE	endothelin-converting enzyme-like 1	F>UF	[17]
NLRR3	neuronal leucine-rich repeat 3	F>UF	[18]
TTL	tubulin tyrosine ligase	F>UF	[19]
BMCC1	novel putative apoptosis-related gene with BCH domain	F>UF	
FOG2	Friend of GATA protein 2	F>UF	[16]
NEDL1	NEDD4-like ubiquitin ligase 1	F>UF	
NEDL2	NEDD4-like ubiquitin ligase 2	F>UF	
GABARAP	gamma-aminobutyric acid receptor-associated protein gene	F>UF	[20]
GABA(A) family	GABA(A) receptor subunit gene family	F>UF	[20]
TRKB	neurotrophic tyrosine kinase, receptor, type 2	F<UF	[4]
hTERT	telomerase reverse transcriptase	F<UF	[5]
NM23A	non-metastatic cells 1 (*NM23-H1*)	F<UF	[12]
NM23B	non-metastatic cells 2 (*NM23-H2*)	F<UF	[13]
BIRC5	baculoviral IAP repeat-containing 5 (survivin)	F<UF	[11]
PPM1D	protein phosphatase 1D	F<UF	[14]
NLRR1	neuronal leucine-rich repeat 1	F<UF	[18]
LMO3	LIM-only protein 3	F<UF	

[a] F;favorable NBL, UF;unfavorable NBL.

the patient. Therefore, additional potent markers for predicting the NBL prognosis should be discovered to construct a more effective as well as less toxic therapeutic strategy. Recent works have demonstrated that cancers can be diagnosed on the basis of gene expression profiling using cDNA microarrays with calculation by computational algorithms. This process needs (1) mass collection or identification of genes expressed in NBLs, (2) construction of a DNA chip and analysis of tumor samples, (3) computational analysis of gene expression data and identification of prognosis-related genes, and (4) conversion of these findings into better diagnosis and treatment. In this review, we discuss the recent attempts of large-scale molecular profiling of NBL and their future applications to the clinic.

2. Prognostic markers for neuroblastoma

In addition to conventional prognostic markers such as age, INSS stage, *MYCN* copy number, histology, and DNA ploidy, expression levels of several genes have recently been added as new indicators. They include inverse relationship of *TRKA* and *TRKB* expression [3,4], *telomerase* [5], *CD44* [6], *pleiotrophin* [7], *N-cadherin* [8], *H-RAS* [9], and *CDC10* [10] (Table 1). From the analyses of genomic aberrations occurred in NBLs, several candidate genes that exhibit overexpression in advanced NBL were identified such as *survivin* [11], *NM23-H1* and *NM23-H2* [12,13], and *PPM1D* [14]. These genes are located on chromosome 17q, which is known to be frequently increased chromosomal copies in advanced NBLs.

3. Identification of novel prognosis-related genes

Various genomic approaches have been used to identify differentially expressed genes among different tissue and tumor types, including differential hybridization screening, representational difference analysis (RDA), gene counting using cDNA libraries followed by semi-quantitative reverse transcriptase polymerase chain reaction (RT-PCR) screening, serial analysis of

gene expression (SAGE), suppression subtractive hybridization (SSH), and cDNA and oligonucleotide microarrays.

In order to collect a large number of genes expressed in various type of NBLs, we have constructed oligo-capping cDNA libraries from primary NBL tissues with different biological characteristics: the tumors with favorable (F; stage 1, single copy of *MYCN*, high *TrkA* expression) and unfavorable (UF; stage 3 or 4, amplification of *MYCN*, no expression of *TrkA*) characteristics and the stage 4 S tumor [15,16]. Ten thousands of clones in total were isolated from those libraries, which corresponded 5,340 independent genes, and approximately 40% of those were shown to contain novel sequences by database search [16]. To identify the genes expressed differentially between the F and UF subsets, all independent clones except housekeeping genes were subjected to semi-quantitative RT-PCR analysis using RNAs obtained from 16 F and 16 UF NBL tissues as templates. From this project, we have identified more than 500 genes differentially expressed between F and UF NBLs. These included many novel genes with unknown functions, including endothelin-converting enzyme-like 1 (*XCE/ECEL1*) [17], neuronal leucine-rich repeat family members (*NLRR1* and *NLRR3*) [18], tubulin tyrosine ligase (*TTL*) [19], novel putative apoptosis-related gene with BCH domain (*BMCC1*, Machida et al., manuscript in preparation), a member of LIM-only protein (*LMO3*) (Aoyama et al., under submission), and NEDD4-like ubiquitin E3 ligase (*NEDL1* and *NEDL2*) (Miyazaki et al., manuscript in preparation) (Table 1). All these genes were analyzed by quantitative real-time RT-PCR method and confirmed to be strongly related to patient prognosis of NBLs. These genes are now being investigated by functional analysis.

Roberts et al. [20] have applied SSH technique to identify potential NBL biomarkers that may improve outcome prediction, and identified differential expression of members of the GABAergic gene family in NBL. They found that low levels of gamma-aminobutyric acid (GABA) receptor-associated protein (*GABARAP*) gene expression predict decreased survival, and that GABA(A) delta receptor subunit gene expression was predictive of a poor outcome among stage 4S patients.

4. Expression profiling of neuroblastomas by microarray approach

Recently, the DNA microarray method has been applied to comprehensively demonstrate the expression profiles of primary NBLs and cell lines (Table 2). The first microarray-based gene expression profiling study of NBL was reported by Khan et al. [21], who demonstrated that the small, round blue-cell tumors (SRBCTs), including NBL, rhabdomyosarcoma, non-Hodgkin lymphoma, and the Ewing family of tumors, which is often present diagnostic dilemmas in clinical practice, could be distinguished on the basis of their patterns of gene expression using artificial neural networks (ANNs). Among these SRBCTs, they showed that 6 of 7 test samples with NBL were classified correctly by using 93 unique genes. Among the 93 classifier genes, 15 genes were highly and specifically expressed in NBLs. This finding is very important when diagnostic tool is going to apply the gene expression data, because it is the first point to be confirmed whether the tumor, which is to be examined, is NBL or not.

Subsequent microarray studies have facilitated class separation of differentiating NBL tumors from poorly differentiated tumors and of high-risk tumors from low-risk tumors. Yamanaka et al. [22] examined 14 NBLs by 23,040 cDNAs microarray, and identified 78 genes whose expression levels were significantly different between differentiating NBLs and poorly differentiated NBLs. The 78 genes included those associated with cell maturation and apoptosis; 15 genes that were up-regulated in stage 4 tumors included those encoding cell adhesion molecules and cytoskeleton proteins. Berwanger et al. [23] examined expression profiles from 94 primary NBL specimens using a 4,608 cDNA human unigene chip. They found 24 significant genes differentially expressed between stage 1 ($n=19$) and stage 4 ($n=21$) *MYCN* non-amplified tumors. Interestingly, a significant percentage of the 24 genes encoded those involved in signaling through the nonreceptor tyrosine kinase Fyn and the actin cytoskeleton. These genes were coordinately down-regulated in advanced stage NBL, both in *MYCN* amplified and nonamplified tumors (Table 2). They also showed that expression of *FYN* predicts long term survival of NBL patients, independently of *MYCN* amplification. Takita et al. [24] performed DNA microarray analysis on 20

Table 2
Differentially expressed genes identified by gene expression profiling using microarray

	Genes identified	Genes on microarray	Sample number	Category
NBL diagnosis				
Khan et al. [21]	15 genes	6,567cDNAs	16 NBLs	For SRBCTs diagnosis *DPYSL4, CDH2, AF1Q, CRMP1, KIF3C, GAP43, MAP1B, RCV1, SFRP1, GATA2, PFN2, FHL1* (highly and specifically expressed in NBLs)
Expression profiling				
Yamanaka et al. [22]	78 genes	23,040 cDNAs	14 NBLs	Differentiating NBLs vs. poorly differentiated NBLs *ITGE, SYP, OLIG2, MADH2, DFFB, CASP8, CASP9* (up-regulated in differentiating NBLs) *CLDN5, CCND1, NFKBIL2* (up-regulated in poorly differentiated NBLs)
Berwanger et al. [23]	36 genes	4,608 cDNAs	94 NBLs	Stage 1 vs. stage 4 *MYCN* non-amplified tumors *FYN, AFAP, CTNNA1, NRCAM, tropomodulin, MARCKS* (down-regulated in advanced stage NBL)
Takita et al. [24]	3 genes	1,700 genes	20 NBLs	Stage 1 vs. stage 4 *BIRC3, CDKN2D* (up-regulated in the early-stage group) *SMARCD3* (down-regulated in the early-stage group)
Hiyama et al. [25]	123 genes	6,272 cDNAs	20 NBLs	Unfavorable vs. favorable (regressing and maturing) 43 genes including *MYCN, hTERT, NME1, CCND1, CCNE1, E1, BIRC5, BIRC1* (up-regulated in unfavorable NBLs) 80 genes (up-regulated in favorable NBLs) *CD44, IGF2, TRKA, ANK1* (highly expressed in maturing NBLs) *CASP8, CASP9, TNFSF10, NGFA, GDF10* (highly expressed in regressing NBLs)
McArdle et al. [26]		14,500 genes	20 NBLs	Differentially expressed in the 11q-, MYCN non-amplified and hyperdiploid subtypes of NBL
Janoueix-Lerosey et al.[27]		320 genes (on 1p35-36)	43 NBLs	1p loss vs. 1p-normal *CDC42, VAMP3, CLSTN1, GNB1, STMN1, RPA2, RBAF600, FBXO6, MAD2L2* (decreased expression in NBLs with 1p deletion)
Prognosis prediction				
Wei et al. [28]	19 genes	42,578 cDNA	56 NBLs	To develop an accurate predictor of survival for patient with NBL *DLK1, PRSS3, ARC, SLIT3, MYCN, JPH1* (up-regulated in the poor-outcome group) *ARHI, CNR1, CD44, ROBO2, BTBD3, KLRC3* (down-regulated in the poor-outcome group)
Ohira et al. [29]	70 genes	5,340 cDNAs	136 NBLs	To develop an accurate predictor of survival for patient with NBL

primary tumors (stage 1 versus 4) and identified that the expression of *BIRC3* and *CDKN2D* genes were significantly higher in the early-stage group than in the advanced-stage group and that the expression of the *SMARCD3* gene was significantly reduced in the early-stage group. The *BIRC3*, *CDKN2D*, and *SMARCD3* genes have been reported to be associated with apoptosis, cell cycles, and the transcriptional activator, respectively. Hiyama et al. [25] analyzed 20 NBLs with 6272 cDNAs microarray, and revealed that 43 genes, including *MYCN*, *hTERT*, *NM23-H1*, cell cycle regulatory protein-coding genes (*CCND1*, *CCNE1*, *E1*), and apoptosis-escape genes (*BIRC5*, *BIRC1*) were highly expressed in unfavorable neuroblastomas, while another 80 genes, including neuronal differentiating genes and apoptotic inducing genes (*CD44*, *IGF2*, *TRKA*, *ANK1* in maturing NBLs, *CASP8*, *CASP9*, *TNFSF10*, *NGFA*, *GDF10* in regressing NBLs) were detected as highly expressed in favorable tumors.

There have been several studies by focusing the certain genomic aberrations and corresponding gene expression profiles. McArdle et al. [26] identified transcripts that are differentially expressed in the 11q-, *MYCN* nonamplified and hyperdiploid subtypes of NBL. Janoueix-Lerosey et al. [27] compared the expression profiles between the tumors with 1p loss and those with normal 1p status and identified the genes with decreased expression in NBLs with 1p deletion (Table 2).

5. Microarray-based system for predicting prognosis of neuroblastoma patients

We now have in our hands the increasing number of information for genes which can distinguish prognosis of the patient with NBL as described above. These data should subsequently be integrated and organized to construct a simple prediction system which is practical for the clinic. Such efforts are now ongoing.

Wei et al. [28] have performed gene expression profiling of 56 NBLs using cDNA microarrays containing 42,578 cDNA clones and used artificial neural networks (ANNs) to develop an accurate predictor of survival for each individual patient with NBL. ANN-based prognosis prediction has been accomplished by using expression levels of only 19 genes including *MYCN* and *CD44*. In addition, these 19 predictor genes were able to additionally classify high-risk patients into two subgroups according to their survival status. Among these predictor genes, *DLK1*, *PRSS3*, *ARC*, *SLIT3*, *MYCN* and *JPH1* were up-regulated in the poor-outcome group included, whereas *ARHI*, *CNR1*, *CD44*, *ROBO2*, *BTBD3* and *KLRC3* were down-regulated.

We also have constructed an in-house, microceramic pump-based ink-jet-printed cDNA microarray carrying 5,340 genes obtained from primary NBL cDNA libraries and applied it for the analysis of 136 tumors. A probabilistic output computational analysis using learning samples has selected 70 genes which constructed a classifier for patient outcome, and provided a correct prognosis of test samples with high efficiency [29]. Of clinical interest, Kaplan-Meier analysis indicated that the classifier can divide significantly 5-year survivals of NBL patients, even for the intermediate risk type. Furthermore, our microarray prediction exhibited the best balance between sensitivity and specificity among prognostic factors including *MYCN* amplification and *TrkA* expression.

These findings provide evidence of a gene expression signature that can predict prognosis independent of currently known risk factors and could assist physicians in the individual management of patients with high-risk NBL. Such gene expression-based diagnosis system should be highly accurate and reproducible, as well as simple, easy to analyze, and with low cost. Based on this, we subsequently made a mini-chip carrying top-ranked 200 genes for clinical use. We are now investigating its (1) reproducibility from the original 5,340 genes chip, (2) potential of predicting prognosis for the newly added test samples, (3) potential of predicting prognosis when whole experimental process (RNA isolation, sample labeling, hybridization, and calculation of the probability of patient survival by using the classifier) is conducted in an independent laboratory. After confirming these, the microarray system will come to prove its practical use to be feasible in the clinic to predict the prognosis of the patient with NBL.

6. Conclusion

Using the gene expression profiling, we are now able to distinguish a group of high-risk patients with high efficiency who will not respond to conventional therapy and therefore require alternative treatment strategies. Although further prospective studies will be necessary, we may also be able to reduce the toxicity of treatment regime for the patients who have been predicted to survive according to gene expression profile. Recently, in addition to the gene expression profiling, certain genome aberrations as well as epigenetic alterations have been reported to be strongly related to the patient prognosis with NBL. Abe et al. [30] indicated that poor NBLs suffer the increased methylation pressure in their tumor genome, and that the methylation of certain CpG island, such as *Protocadherin beta* family, can predict poor NBL prognosis with high sensitivity. Furthermore, screening of prognosis-related proteins secreted into serum of NBL patients has been started by many groups. Combination of such independent systems to predict

prognosis will further improve the accuracy of the diagnostic system for NBL.

Acknowledgements

This work was supported in part by a fund from Hisamitsu Pharmaceutical Co., Inc. and by Grant-in-Aids for Scientific Research on Priority Areas (C) 'Medical Genome Science' and 'Genome Information Science', and for Scientific Research (B) from the Ministry of Education, Culture, Sports, Science and Technology of Japan, and by Grant-in Aids for Cancer Research and for the 2nd Term Comprehensive 10-year Strategy for Cancer Control from the Ministry of Health, Labour and Welfare of Japan.

References

[1] R.P. Bolande, The neurocristopathies: a unifying concept of disease arising in neural crest maldevelopment, Hum. Pathol. 5 (1974) 409–429.
[2] J.L. Weinstein, H.M. Katzenstein, S.L. Cohn, Advances in the diagnosis and treatment of neuroblastoma, Oncologist 8 (2003) 278–292.
[3] A. Nakagawara, M. Arima-Nakagawara, N.J. Scavarda, C.G. Azar, A.B. Cantor, G.M. Brodeur, Association between high levels of expression of the TRK gene and favorable outcome in human neuroblastoma, N. Engl. J. Med. 328 (1993) 847–854.
[4] A. Nakagawara, C.G. Azar, N.J. Scavarda, G.M. Brodeur, Expression and function of TRK-B and BDNF in human neuroblastomas, Mol. Cell Biol. 14 (1994) 759–767.
[5] E. Hiyama, K. Hiyama, T. Yokoyama, Y. Matsuura, M.A. Piatyszek, J.W. Shay, Correlating telomerase activity levels with human neuroblastoma outcomes, Nat. Med. 1 (1995) 249–255.
[6] M.C. Favrot, V. Combaret, C. Lasset, CD44–a new prognostic marker for neuroblastoma, N. Engl. J. Med. 1993; 329.
[7] A. Nakagawara, J. Milbrandt, T. Muramatsu, T.F. Deuel, H. Zhao, A. Cnaan, G.M. Brodeur, Differential expression of pleiotrophin and midkine in advanced neuroblastomas, Cancer Res. 55 (1995) 1792–1797.
[8] R. Shimono, S. Matsubara, H. Takamatsu, T. Fukushige, M. Ozawa, The expression of cadherins in human neuroblastoma cell lines and clinical tumors, Anticancer Res. 20 (2000) 917–923.
[9] T. Tanaka, T. Sugimoto, T. Sawada, Prognostic discrimination among neuroblastomas according to Ha-ras/trk A gene expression: a comparison of the profiles of neuroblastomas detected clinically and those detected through mass screening, Cancer 83 (1998) 1626–1633.
[10] T. Nagata, Y. Takahashi, S. Asai, Y. Ishii, H. Mugishima, T. Suzuki, et al., The high level of hCDC10 gene expression in neuroblastoma may be associated with favorable characteristics of the tumor, J. Surg. Res. 92 (2000) 267–275.
[11] A. Islam, H. Kageyama, N. Takada, T. Kawamoto, H. Takayasu, E. Isogai, et al., High expression of Survivin, mapped to 17q25, is significantly associated with poor prognostic factors and promotes cell survival in human neuroblastoma, Oncogene 19 (2000) 617–623.
[12] N. Hailat, D.R. Keim, R.F. Melhem, X.X. Zhu, C. Eckerskorn, G.M. Brodeur, et al., High levels of p19/nm23 protein in neuroblastoma are associated with advanced stage disease and with N-myc gene amplification, J. Clin. Invest. 88 (1991) 341–345.
[13] A. Leone, R.C. Seeger, C.M. Hong, Y.Y. Hu, M.J. Arboleda, G.M. Brodeur, et al., Evidence for nm23 RNA overexpression, DNA amplification and mutation in aggressive childhood neuroblastomas, Oncogene 8 (1993) 855–865.
[14] F. Saito-Ohara, I. Imoto, J. Inoue, H. Hosoi, A. Nakagawara, T. Sugimoto, J. Inazawa, PPM1D is a potential target for 17q gain in neuroblastoma, Cancer Res. 63 (2003) 1876–1883.
[15] M. Ohira, A. Morohashi, Y. Nakamura, E. Isogai, K. Furuya, S. Hamano, et al., Neuroblastoma oligo-capping cDNA project: toward the understanding of the genesis and biology of neuroblastoma, Cancer Lett. 197 (2003) 63–68.
[16] M. Ohira, A. Morohashi, H. Inuzuka, T. Shishikura, T. Kawamoto, H. Kageyama, et al., Expression profiling and characterization of 4200 genes cloned from primary neuroblastomas: identification of 305 genes differentially expressed between favorable and unfavorable subsets, Oncogene 22 (2003) 5525–5536.
[17] T. Kawamoto, M. Ohira, S. Hamano, T. Hori, A. Nakagawara, High expression of the novel endothelin-converting enzyme genes, Nbla03145/ECEL1alpha and beta, is associated with favorable prognosis in human neuroblastomas, Int. J. Oncol. 22 (2003) 815–822.
[18] S. Hamano, M. Ohira, E. Isogai, K. Nakada, A. Nakagawara, Identification of novel human neuronal leucine-rich repeat (hNLRR) family genes and inverse association of expression of Nbla10449/hNLRR-1 and Nbla10677/hNLRR-3 with the prognosis of primary neuroblastomas, Int. J. Oncol. 24 (2004) 1457–1466.
[19] C. Kato, K. Miyazaki, A. Nakagawa, M. Ohira, Y. Nakamura, T. Ozaki, et al., Low expression of human tubulin tyrosine ligase and suppressed tubulin tyrosination/detyrosination cycle are associated with impaired neuronal differentiation in neuroblastomas with poor prognosis, Int. J. Cancer 112 (2004) 365–375.
[20] S.S. Roberts, M. Mori, P. Pattee, J. Lapidus, R. Mathews, J.P. O'Malley, et al., GABAergic system gene expression predicts clinical outcome in patients with neuroblastoma, J. Clin. Oncol. 22 (2004) 4127–4134.